Electronics **2014**, *3*, 132-164; doi:10.3390/electronics3010132

OPEN ACCESS

electronics

ISSN 2079-9292

www.mdpi.com/journal/electronics

Review

Electron and Hole Transport Layers: Their Use in Inverted Bulk Heterojunction Polymer Solar Cells

Sandro Lattante

Dipartimento di Matematica e Fisica "Ennio de Giorgi", Universitá del Salento, via per Arnesano, Lecce 73100, Italy; E-Mail: sandro.lattante@unisalento.it.

Received: 8 January 2014; in revised form: 19 February 2014 / Accepted: 24 February 2014 / Published: 6 March 2014

Abstract: Bulk heterojunction polymer solar cells (BHJ PSCs) are very promising organic-based devices for low-cost solar energy conversion, compatible with roll-to-roll or general printing methods for mass production. Nevertheless, to date, many issues should still be addressed, one of these being the poor stability in ambient conditions. One elegant way to overcome such an issue is the so-called "inverted" BHJ PSC, a device geometry in which the charge collection is reverted in comparison with the standard geometry device, *i.e.*, the electrons are collected by the bottom electrode and the holes by the top electrode (in contact with air). This reverted geometry allows one to use a high work function top metal electrode, like silver or gold (thus avoiding its fast oxidation and degradation), and eliminates the need of a polymeric hole transport layer, typically of an acidic nature, on top of the transparent metal oxide bottom electrode. Moreover, this geometry is fully compatible with standard roll-to-roll manufacturing in air and is less demanding for a good post-production encapsulation process. To date, the external power conversion efficiencies of the inverted devices are generally comparable to their standard analogues, once both the electron transport layer and the hole transport layer are fully optimized for the particular device. Here, the most recent results on this particular optimization process will be reviewed, and a general outlook regarding the inverted BHJ PSC will be depicted.

Keywords: polymer solar cell; inverted bulk heterojunctions

---

1. Introduction

In 1977, Shirakawa, Louis, MacDiarmid, Chiang and Heeger reported on their discovery of electrically conductive polymers [1] (for which, in 2000, the Nobel Prize in Chemistry was awarded

jointly to Heeger, MacDiarmid and Shirakawa). From that milestone, a great deal of research activity on conjugated polymer-based optoelectronics has been developed all over the world. To date, organic-based light-emitting diodes (OLED) have become commercially available with good performance, and polymer-based photovoltaics has reached high efficiency: over 9% in lab-scale devices [2,3]. The exploiting of the peculiar properties of conjugated polymers in the photovoltaic (PV) field is more recent than in light emitting devices, and still, a lot of unsolved questions must be addressed in order to really develop a commercial route for polymer PV [4]. Following the ideas and the experimental results in the pioneering works on small organic molecule-based photovoltaics [5], in 1993, Sariciftci reported on the evidence of a conjugated polymer/fullerene heterojunction bilayer solar cell [6,7]. Soon after that, the first polymeric *bulk*heterojunction (BHJ) PV device was described by Yu *et al*. [8]. In 1995, the new soluble fullerene derivatives [9] allowed the boosting of device performances [10]. Starting from those first works, a lot of efforts have been made in order to increase the device power conversion efficiency (PCE) and stability, mainly working on synthesizing new polymers to be used in the active layer and on optimizing the device structure and geometry. The most commonly used device structure for a BHJ organic solar cell comprises a conductive transparent substrate—typically metal oxides, like indium tin oxide (ITO) or fluorine-doped tin oxide (FTO) on glass or plastic substrates—covered by a thin hole conducting layer, such as the polymer, poly(3,4-ethylenedioxythiophene)-poly(styrenesulfonate) (PEDOT:PSS), over which, the active layer is deposited, typically from a solution by means of spin coating, doctor blading, ink-jet printing, spray coating, *etc*. [11–14]. Finally, a thin metal layer is realized (Al, Ca/Al, LiF/Al, for instance), usually by thermal evaporation. This structure has been used in the realization of devices with very good performance, reaching a PCE of around 9% [3]. Despite these good efficiency reports, which, anyway, are far from being general and reproducible [4], such a structure suffers from several drawbacks: due to the required energy level alignment among all the cell components, a low work function metal electrode must be used on top of the device for the electron extraction, like Al. However, low work function metals undergo very fast oxidation when exposed to air, losing their conductivity, suddenly turning a working device into a faulty one. Moreover, the PEDOT:PSS is acidic in nature and is thus detrimental to the underlying metal oxide layer, which undergoes fast degradation [15,16]. Finally, it has been widely reported that polymer/fullerene (as well as polymer/polymer blends [17]) are characterized by a stratified composition (vertical phase separation) during the film formation [18], with the fullerene phase—that is, the electron-conducting phase—mainly concentrated at the bottom of the film and the polymer phase—the hole-conducting one—concentrated mainly at the top of the film. Thus, the film vertical phase structure is opposite to the ideal one, where the electron-conducting phase must face the top low-work function electrode and the hole-conductive phase must face the bottom high work function electrode. All these problems can be avoided by reversing the collection process, *i.e.*, collecting the holes by the top electrode and the electrons by the bottom electrode. In such a structure, the top metal electrode would be a high work function electrode, like silver or gold (Ag or Au), thus eliminating the oxidation problem, while the bottom electrode should be a transparent electron conducting layer (oxides, like zinc oxides (ZnO) or titanium oxide (TiO_x) are good examples), eliminating the problem of the acidic PEDOT:PSS on ITO or FTO.

This inverted structure was first exploited in the fabrication of organic light emitting diodes, also initially referred to as an "upside-down" structure [19]; then, it started to be exploited also in the PV field [20,21].

After these pioneering works, it has been demonstrated that the inverted structure allows one to reach performances even better than the standard one [22,23]. Despite this, the research on inverted polymer solar cells (PSCs) is a very small fraction of the total research in the PSC field. As of November 14, 2013, a simple search on the ISI Web of Knowledge using as key words "bulk heterojunction solar cell" (excluding the word "inverted") gives about 7400 papers, while when the key words "inverted" AND "bulk heterojunction solar cell" are used, only 207 results are shown, that is less than 3% of the published papers. The situation does not change much if the search string is not limited to bulk heterojunction, but to the more generic "polymer solar cell" (24,700 results) to be compared with the very small number of 514 results when searching for "inverted" AND "polymer solar cell" (less than 2% of the published papers on polymer solar cell), nor would a great variation of this ratio come out if the search were limited to the last two years. This was already pointed out by Krebs and coworkers very recently [4] (they estimated that less than 10% of published results were focused on the inverted structure). This is quite surprising, since the polymeric bulk heterojunction inverted solar cell (BHJ ISC) has by far better stability over time than the standard geometry devices [24].

Among these relative few papers, the review articles are very limited. The most recent and complete, by Zhang *et al*., published in 2011 [25], however, reviews general inverted organic devices, not focusing particularly on the polymer bulk heterojunction concept; while in the one by Hau *et al*. [24], published in 2010, there is no general focus on the electrode interfaces.

The aim of this review is to present a comprehensive description of the most recent results on the improvement in the performances of hole transport layers (HTLs) and electron transport layers (ETLs) used in BHJ ISC in order to tentatively give a strong baseline for further research directions and improvements. On the contrary, this paper will not consider: (1) small molecule-based devices; (2) bi-layered active materials or multi-layered active material devices; and (3) tandem devices; for all of which, there is an excellent scientific literature.

The paper will be structured as follows: first, a very brief and general overview of the working principles of the bulk heterojunction solar cell is given; then, a comparison between the standard geometry device and the inverted one is sketched, highlighting the pros and cons of both, following a detailed review of the various materials and strategies for optimizing the hole transport layer (HTL) and the electron transport layer (ETL); finally, a summary of the major findings is given.

2. The Bulk Heterojunction Solar Cell: Working Principles

The working principle of a polymer BHJ solar cell (see Figure 1) could barely be summarized as the creation of an exciton in the active layer, due to light absorption, and the separation of this exciton into two separate charge carriers at the interfaces between the species that constitute the active layer (typically, a binary blend of a polymer and a fullerene or two polymers, which act as the donor phase and the acceptor phase), with subsequent collection by the electrodes [26]. Despite their apparent simplicity, all of these steps must obey very strict limitations in order to be as efficient as one would need. First of

all, the generated excitons must hop between the molecules reaching an interface between the two phases before recombining (radiatively or non-radiatively). This means that the two phases should be mixed in an optimal structure, with phase domains usually in the order of 10–30 nm (the average exciton diffusion length in polymers [26]). Then, the position of the energy levels at the interface must be favorable for a fast exciton dissociation followed by charge separation (*i.e.*, the electron in the acceptor phase and the hole in the donor phase without successive recombination [26]). After that, the charges must travel inside the respective phases, reaching the collecting electrodes again without a charge recombination: at this point, the energetic level structure at the electrode interfaces plays a fundamental role, ideally the interface being an ohmic contact [26].

Figure 1. Schematic basic working principle of a polymeric bulk heterojunction solar cell.

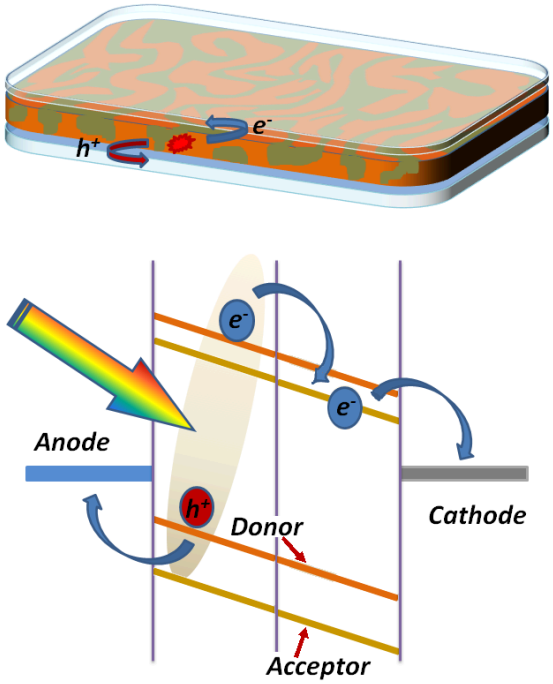

The standard geometry device is sketched in the upper part of Figure 2; as already mentioned in the Introduction, it typically consists of a transparent bottom electrode for the hole collection, a thin layer of active material and a top metal electrode for the electron collection. In the inverted structure (bottom of Figure 2), the role of the electrodes is swapped; thus, the electrons are collected by the bottom transparent electrode and the holes by the top metal electrode. This reversed collection implies that the work function of the top electrode must be high enough in order to match the donor highest occupied molecular orbital (HOMO) energy level, and the work function of the bottom electrode must be low enough in order to match the acceptor lowest unoccupied molecular orbital (LUMO) energy level. If the requirement of the top metal electrode can be simply fulfilled by selecting high work function metals, like gold or silver, the right selection of the bottom electrode is more tricky. In fact, the most used transparent metal oxides, like ITO or FTO, possess high work functions that do not match well with the LUMO level of the acceptors. The matching of the energy levels is obtained by modifying the bottom electrode with the deposition of

a thin layer of suitable electron conducting (hole blocking) materials, like, for instance, ZnO or TiO_x, which are, moreover, transparent to visible light. The effects of this electrode capsizing are multiple, and the working properties of the devices are strongly influenced, as will be described in the following sections.

Figure 2. Schematic geometry for (**top**) a standard bulk heterojunction (BHJ) device and (**bottom**) an inverted BHJ device. The main component layers are sketched. ETL, electron transport layer; HTL, hole transport layer.

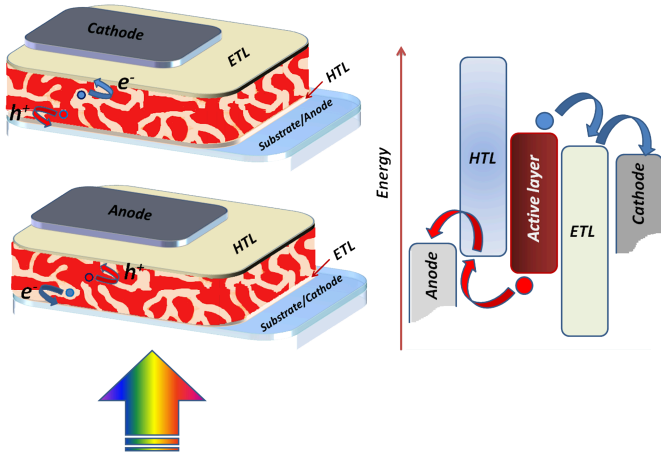

2.1. Light Absorption and Electromagnetic Field Distribution: Comparison between Standard and Inverted Structure

The processes of exciton diffusion, exciton dissociation and charge separation, as well as charge recombination in the bulk active layer depend on the active layer properties and are thus expected to be the same for both of the structures. On the contrary, standard and inverted structures present strong differences in the electromagnetic field distribution inside the device.

The main criterion that should be fulfilled in every PV device is that the solar light should be well absorbed by the active layer (that means that, ideally, the main part of the solar spectrum reaching the Earth's surface should be harvested). This is not a well-solved issue yet in organic PV, since each polymer absorbs a narrow range of visible light, and typically, the ones used in BHJ solar cells have no or low absorption in the low energy side of the solar spectrum. Since the open circuit voltage (V_{oc}) of a BHJ PSC is believed to be determined mainly by the donor HOMO-acceptor LUMO energy gap [26], the exploitation of low band-gap donors typically decreases the V_{oc}, and a trade-off must be reached between good light harvesting and good electrical parameters. Although this is a problem that affects both the standard geometry and the inverted one, it has been demonstrated that the inverted configuration better harvests the incoming light, due to a more favorable electromagnetic field distribution inside the active layer. In fact, Ameri *et al.* [22] considered a poly-3-hexyl thiophene (P3HT):phenyl-C61-butyric acid methyl ester (PCBM) standard geometry solar cell and an inverted analogue; they found that the inverted device performed about 15% better than the standard one. In order to understand the reasons underlying the better performance, they optically modeled the devices. They found that in the inverted structure, the number of absorbed photons by the active layer was increased, thus resulting in an increased number of

charge carriers, thanks to the use of a TiO_x bottom layer, which is transparent to visible light, instead of a PEDOT:PSS layer, which absorbs about 20% of the incoming light. With these observations, they were able to explain roughly a 10% increase in performance. The remaining 5% boost was instead ascribed to an unbalanced electron and hole mobilities that lead to a more efficient charge collection in the inverted structure than in the standard one. Indeed, assuming an exponential absorption profile, the charge carriers are generated mainly closer to the bottom electrode rather than to the top metal electrode; thus in the presence of unbalanced mobilities with the hole mobility lower than the electron one, a better charge collection is expected in the inverted configuration. What was still missing in the discussion was the findings that the P3HT:PCBM blend undergoes a vertical phase separation during the process of film formation, resulting in a stratified structure in which a PCBM-rich layer is formed on the bottom of the film and a P3HT-rich layer is formed on the top [18] (see Figure 3). As the electrons mainly travel inside the PCBM phase and the holes mainly travel inside the P3HT phase towards the respective electrodes, the inverted configuration is the best one, being characterized by a self-assembled ETL (hole blocking) at the electron extraction electrode (bottom) and a HTL (electron-blocking) at the hole extraction electrode (top), thus both increasing the charge extraction efficiency and reducing the bimolecular recombination at the electrodes.

Figure 3. Vertical phase separation in a BHJ polymer solar cell (PSC). Reprinted with permission from [18]. PCBM, phenyl-C61-butyric acid methyl ester; PEDOT:PSS, poly(3,4-ethylenedioxythiophene)-poly(styrenesulfonate).

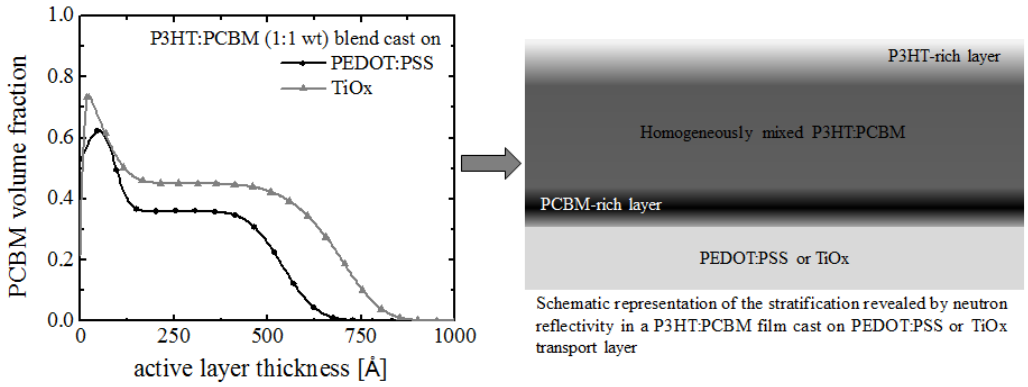

These findings were partially confirmed by Chen *et al.* [27], who modeled a P3HT:PCBM-based inverted device both optically and electrically. They concluded that if one considers only the optical aspects of the structure (*i.e.*, the field distribution inside the active layer), the inverted structure should be better performing than the standard one for the major part of the considered active layer thicknesses. The standard device should, on the contrary, perform better when the active layer thickness is just the ideal one for constructive interference inside the film between the incoming radiation and the reflected one from the top metal electrode. Concerning the electrical aspects, the electrical behavior of the device was modeled as a function of the charge drift length, L, a parameter that accounts for the charge lifetime and mobility, being defined as the maximum length that a charge carrier can drift within its lifetime before any possible recombination. The value of L influences the electromagnetic field distribution and the optical modulation inside the active layer for each thickness. They showed that the inverted structure

is better than the standard one, only if the active layer thickness is comparable with L, while the standard geometry performs better if the active layer thickness is greater than L. This is due to the fact that L induces an "effective area" inside the active layer where the absorbed photons are efficiently transformed into charge carriers, while photons absorbed outside this area are mainly lost, not contributing to the photocurrent. Since the position of this effective area depends on the different charge transport properties peculiar to the active material, the optical field modulation inside the device together with the position of the effective area determine the performance differences between standard and inverted geometry.

This prediction, however, was slightly in contrast with the results of Aziz, Li and coworkers [28], who showed a remarkable difference between standard and inverted devices, especially when analyzing the short circuit current density, J_{sc}. In both devices, the J_{sc} increased with increasing the thickness of the active layer, but in their case, the J_{sc} in the standard device started to decrease for an active layer thicker than 300 nm, while the J_{sc} in the inverted one remained constant. They explained their results with a reduced recombination mechanism in the inverted structure (coherently with the conclusions of Ameri *et al.* [22]) and a reduction of the series resistance in the inverted device. This apparent contrast could be, however, explained with the differences in the device structure considering the nature, properties and thicknesses of all the constituent layers, which strongly influence the optical and electrical properties [27].

Even if those reports were based on a P3HT:PCBM active layer, many other research groups reported improved performances of the inverted structure compared to the standard analogue when other active materials were used. For instance, Ma *et al.* reported a boost in performances for an inverted device based on a blend of PBDT-12/PyT2 [23].

Overall, from both the optical and electrical analyses given by those reports, it appears clear that the inverted structure has many advantages with respect to the standard one, at least when thin layers are used, which is actually the standard in realizing organic-based optoelectronic devices. Given the general behavior of the devices, in the next sections, a description of the most recent results for the electrode interfaces is given.

3. ETLs and HTLs: Recent Developments

In both the standard and inverted devices, the active material plays the same role, that is, in short, to absorb photons and to convert them into free charge carriers (the influence of optical and electrical parameters on this process has been briefly sketched in the previous section). In order to achieve good performances, however, it is mandatory that a BHJ comprises both an HTL and an ETL.

A list of requirements that a good ETL, as well as a good HTL should fulfill (among which are transparency, good electrical properties and chemical stability) is given in a recent review on the synthesis methods of metal oxides by Litzov and Brabec [29]; although that review focuses on metal oxides only, the general list applies to every material to be used as the electron or hole-transport layer in a BHJ ISC. Here, a summary on the most recent results about different class of materials for the realization of the various ETLs and HTLs in BHJ ISCs is given.

3.1. Bottom Electrode: Electron Collection

The main requirements for the bottom electrode are a good electron transport property and, when the light is collected through it, transparency to the solar radiation. This limits the choice to a few materials, among which are the well-known and widely-used ZnO and TiO_x [29] (which have also a good electronic level matching with the LUMOs of most of the polymers used in PV), other less used materials, like Cs_2CO_3 [30], and new polymeric materials, like poly(2-(dimethylamino)ethyl methacrylate) (PDMAEMA) [31] and PFEN-Hg [32]. The various realization methods of transparent metal oxides have been described in great detail in a very recent review [29]. In the present work, the attention will be focused on the effects of the ETL and HTL layer properties on the device performances.

3.1.1. ZnO

Very thin layers of ZnO are easily realized by means of several deposition techniques, like sol-gel [33], spray-coating [34] and nanoparticle (NP) deposition [35]. Most of the time, the as-deposited film needs a process of annealing usually at high temperatures in order to optimize the crystalline structure [36], but also, low annealing temperature processes have been recently reported [35,37,38].

Considering the P3HT:PCBM-based devices just as a prototypical PV system, the overall reported power conversion efficiency using ZnO as the ETL spans from about 2% to about 4% [29,35,39]. This quite wide range is due to the differences in several factors, including the chosen HTL, the parameters involved in the active blend preparation and optimization and the properties of the ZnO ETL layer. In this section, the attention will be focused on the possible influences of the ETL layer on the device performances with various active layers.

One of the most important parameters that determines the overall performances of the device is the morphology (and consequently, the roughness) of the ZnO layer. Despite the several methods developed to deposit a thin ZnO layer on substrates, there is no "elective" method to obtain the optimal morphology; each method can afford the best results, once all the deposition parameters have been optimized. Yu *et al*. [40] showed that the power conversion efficiency of a P3HT:PCBM-based ISC was increased from 2.08% to 2.88% by increasing the surface roughness of the ZnO layer. Since the ZnO film realized by the sol-gel technique is affected by three processes during the annealing [41] (solvent evaporation, zinc acetate decomposition and crystallization), they changed the surface roughness of the layer by simply varying the annealing rate of the as-deposited (by sol-gel) ZnO layer, namely a slow annealing rate of 9 °C/min and a fast one of 56 °C/min up to 300 °C. They found both an increase in J_{sc} and in FF for the slowly annealed sample. The boost in the J_{sc} was explained by the enhanced light absorption, due to the rougher ZnO surface, which should provide an efficient light trapping mechanism: once being scattered by the ZnO layer, the light is reflected back by the upper Ag electrode in multiple directions, thus increasing the path length inside the active layer. The higher FF was explained considering the better crystallization of the ZnO, due to the slow annealing rate, which resulted in a more effective electron extraction and hole blocking (it is known that FF is strongly related to the charge extraction efficiency at the interfaces [42]). Dhibi *et al*. [43] reported the same conclusions in a PCDTBT:PC70BM-based ISC: the absorption of the blend cast onto the ITO/ZnO (sol-gel) substrate was higher than that of the one cast onto the bare ITO substrate. This effect was ascribed both to the light scattering mechanism, as well as to

the larger surface area between the ZnO and the active blend. However, they noted that a too pronounced roughness of the sol-gel-derived ZnO films could be, on the other hand, detrimental to the overall device performance when a very thin active layer is needed (that is the case of the PCDTBT:PC70BM blend), due to the rising-up of a high contact resistance and a large leakage current [44]. Moreover, they demonstrated that also the annealing temperature is a key factor in order to determine the morphology of the layer: they annealed the ZnO films at three different temperatures, namely 130 °C, 150 °C and 200 °C, and characterized them by photoluminescence and Raman measurements, showing that the 150 °C annealed film was affected by better crystallization, which could enhance the electron extraction and mobility, as well as suppress the leakage current into the device. Vijila and coworkers [45] showed that the annealing temperature greatly affects the overall crystalline morphology of the ZnO layer. They demonstrated that a ZnO film annealed at 240 °C was characterized by a higher crystallinity compared to a similar layer, but annealed at 160 °C. The device incorporating the 240 °C annealed ZnO layer performed better (with a 40% higher PCE) than the device realized with the 160 °C annealed ZnO layer. They explained these results, observing that the ZnO layer annealed at 240 °C was characterized by a lower trap depth, thus reflecting in higher charge mobility and better ohmic contact and, consequently, higher J_{sc} and V_{oc}.

These results indicate that both the annealing temperature and the annealing rate should be taken into account in order to optimize both the crystalline structure and the surface roughness of sol-gel-derived ZnO films, looking for a trade-off between increased light scattering by the surface roughness (thus enhancing the active layer absorption, and, hence, the J_{sc}, and increasing the FF, due to the higher interface contact and charge extraction efficiency) and the crystal structure (better charge transport).

A further interesting contribution on this topic is the work by Hu *et al*. [46], showing that the ZnO morphology can also depend on the layer thickness. They realized ZnO layers by the metal organic chemical vapor deposition (MOCVD) technique, finding that the ZnO layer thickness did not influence the energy level alignment at the interfaces, but it had a strong impact on the crystal structure and, hence, on the electrical properties. In particular, with the increase of the thickness, the morphology of the ZnO layer changed from a pure smooth sphere-like structure for a thickness of $<$100 nm to a rough pyramid-like structure starting from 100 nm and above. They indirectly confirmed the above picture of the need for a trade-off between roughness and crystal structure; in fact, they showed that initially, an increase of the ZnO layer thickness, and hence, of the surface roughness, was beneficial for ISC performances (with PCE increasing from 1.60% for 40 nm of ZnO to 2.93% for 80 nm ZnO), while the PCE started to decrease for the thicker ZnO layer (ISCs were based on the P3HT:PCBM active layer).

It is noteworthy that the above results are commonly characterized by the use of no annealing or a relative low post deposition annealing temperature in order to obtain a good overall film morphology. This is quite different from the most commonly used high temperature post deposition annealing process; for example, Park *et al*. [47] used a temperature of 450 °C for annealing a sol-gel-derived ZnO layer to be used as the ETL in a P3HT:PCBM- and a P3HT:PCBM:polyoxyethylene tridecyl ether (PTE)-based device; they demonstrated by XRD that the so-annealed film showed two strong crystalline peaks at 30.3 °(100) and 34.3 °(002). .

Nanostructured ZnO layers also appear to be promising as efficient ETL in ISC. Simple ZnO nanoparticles (NPs) are easily deposited onto substrates by spin coating [35,48] or slot-die

coating [49]: Alstrup *et al.* [49] realized layers of ZnO starting from an aluminum-doped ZnO NP ink using a roll-to-roll compatible method, the slot-die coating. Their results showed that a very efficient ISC can be realized using low-cost techniques that are feasible for large area device realization, once each layer deposition's parameter has been optimized. Regarding the ZnO layer, they also showed that the overall PCE of the final device is correlated with the thickness of the ZnO layer itself. Ibrahem *et al.* [35] prepared thin layers of ZnO NPs using a simple method that avoids the use of any surfactants in order to stabilize the ZnO particles in solutions, simply dispersing ZnO powder in pure ethylene glycol followed by high energy ball milling at room temperature in a batch-type grinder. They showed that the ZnO particle size decreased with the increasing of the grinding time down to an average particle diameter of 25 nm. The NPs, after grinding, were stable in solution without any precipitation, obtaining very uniform and thin films upon spin coating and final device PCEs over 3.5%. Our group realized all polymer ISC using a thin layer (about 80 nm) of ZnO on fluorine-doped tin oxide (FTO) by simply spin coating a commercial (Sigma Aldrich, St. Louis, MO, USA) aqueous dispersion of ZnO NPs with an average diameter less than 100 nm [50], without any post deposition annealing process. The layer morphology resulted in a very uniform sphere-like texture (see Figure 4) without any cracking or pinholes, with an average surface roughness of 4.53 nm. Thus, it is demonstrated that ZnO NP dispersion in water or common organic solvents can be a convenient and roll-to-roll compatible method for obtaining good ZnO ETLs for efficient inverted solar cells.

Figure 4. 1 μm $\times$ 1 μm atomic force microscopy image of ZnO film on a fluorine-doped tin oxide (FTO) substrate by spin coating from a ZnO nanoparticle (NP) aqueous dispersion.

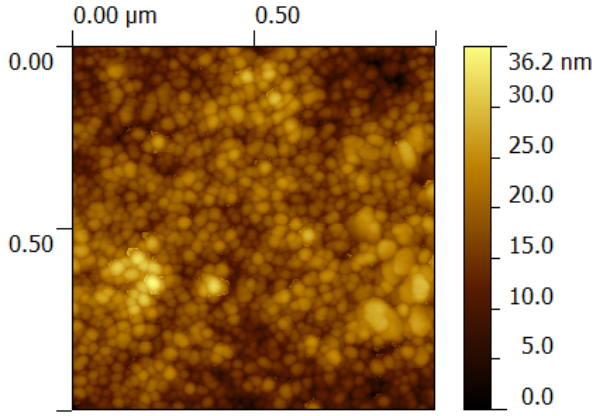

More complex structures have also been reported, like vertically aligned, one-dimensional nanostructures [51] and bi-dimensional nanowalls [52]. The latter, in particular, should theoretically perform better than one-dimensional structures, since it provides a higher contact surface between the ZnO and the active layer (Figure 5). Liang *et al.* [52], however, showed that when compared with ZnO nanorods, the NWs structure does not perform clearly better. They tried to explain their results, observing that the overall growth condition and, hence, the surface chemistry of the two structures are different, thus implying a possible different mechanism of charge recombination and charge transfer through the surface. Nevertheless, their report is quite recent, and there is no systematic optimization of the ZnO NW layer parameters, such as the thickness, etching process and interface modification, in

order to improve and promote the diffusion of the active blend inside the nanostructures, thus leaving a large amount of room for future improvement. Electrospun ZnO nanowires (NWs) were incorporated by Vijila *et al.* [53] in a sol-gel-derived ZnO layer to be used as the ETL in ISCs. With the NW plantation, the overall device performance was increased compared to a control device without NW. This was due to a higher FF (both lower series resistance and higher shunt resistance), as well as a beneficial effect on the active layer phase separation morphology (which was reflected in a higher carrier lifetime and a reduced charge recombination).

A proper doping of the ZnO layer [54,55] is another possible route to improve the charge collection efficiency and to reduce the charge recombination, due to charge trapping by defects or oxygen ions [29]. Hu *et al.*, in the already cited work [46], reported an improved overall performance of an ISC when the intrinsic ZnO (i-ZnO) was doped with boron during the MOCVD process, in particular showing that the J_{sc} increased up to 11.31 mA cm^{-2} when the diborane flow rate was kept at 3 sccm. They explained the results considering a better charge collection at the electrodes (the average resistivity of the ZnO layer decreased from 4.04 $\times$ 10^5 Ω/sq of the i-ZnO to 2.46 $\times$ 10^3 Ω/sq of the best boron-doped ZnO). Alstrup *et al.* [49] doped ZnO with Al in order to improve the conductivity and quality of the ZnO film deposited by the slot-die coating method. Lithium fluoride (LiF) has been used for a long time as an ultra-thin layer underlying the top Al electrode in standard configuration bulk heterojunction solar cells, since it improves device performances [56] and device stability [57]. Chang *et al.* [58], on the contrary, used it for doping a sol-gel-derived ZnO ETL to be used in ISCs based on a P3HT:PCBM active blend, demonstrating an improvement of the overall PCE of the device from 2.9% to 3.3%. Optimized LiF-doped ZnO showed a very high electron mobility up to 11.2 $cm^2V^{-1}s^{-1}$. They concluded that Li atoms occupy interstitial sites, producing electrons, which results in higher electron mobility. At the same time, F atoms occupied in substitutional oxygen sites reduce the oxygen vacancies in the structure and lower the absorption in the visible region. Their conclusions are indeed supported by the fact that the better performance of the device is correlated with an increase in the J_{sc}, all the other cell parameters being almost unchanged.

Figure 5. SEM images of (**A**) the ZnO seed layer, (**B**) the as-grown dense ZnO rods, (**C**) the etched ZnO nanowalls and the (**D**) cross-section of the nanowalls. Reprinted with permission from [52].

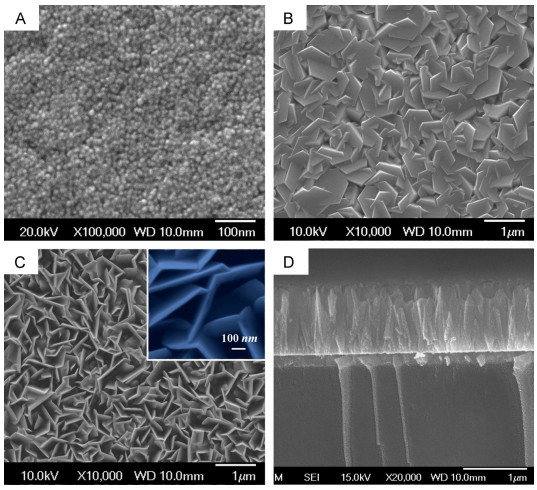

Finally, Du *et al.* [59] showed that UV irradiation of a sol-gel-derived ZnO layer used as the ETL in PBDTTT-C:$PC_{71}BM$-based ISC improved the device performance, due to the increase of the layer conductivity following the reduction of hole traps on ZnO. This is clearly reflected in the higher FF related to a decrease of the device series resistance. The drawback of UV irradiation consisted, however, in a gradual degradation of the polymeric active blend; so, they concluded that, practically, a trade-off between the early stage advantage of UV irradiation and long-term disadvantage due to polymer degradation should be considered in ISCs comprising a ZnO ETL.

Despite the several techniques and the different processes used to date for optimizing ZnO properties, it appears that the final device performance does not depend as much on the technique used for realizing the ZnO layer, but rather on the inner properties of the layer itself, such as the roughness and crystalline structure, both almost independent of the particular deposition method, once optimized.

3.1.2. TiO_x

Although porous crystalline TiO_2 is the standard charge transport layer used in the so-called dye-sensitized solar cell (Grätzel cell) [60], it is, on the contrary, not well suited as the ETL in BHJ ISCs, due to the difficult and tricky deposition of a uniform and homogeneous layer on standard ITO substrates [61,62]. Nevertheless, it has been used by Peng *et al.* [63] in ISCs, showing, in particular, that the overall power conversion efficiency of the device strongly depends on the TiO_2 crystalline structure. When the film is characterized by a well-defined morphology (the homogeneity of nanoparticle shapes and distribution) and a maximum crystal size of about 50 nm, the interface between the TiO_2 and the active material is characterized by an optimal morphology and interaction, thus favoring both exciton dissociation and charge separation, with improved FF (which means less charge recombination and improved charge transport through the inorganic layer).

However, amorphous TiO_x ($x \leq 2$) is as good as crystalline TiO_2 as the ETL, once optimized [64]. Moreover, it is as good as ZnO as the ETL in ISCs, since it is characterized by high electron mobility and high transparency in the visible range [65]. Hadipour *et al.* [66] showed that it is possible to realize a TiO_x ETL layer at room temperature from solution without any post deposition annealing process. They demonstrated that such a layer was as good as calcium in extracting electrons from a bulk heterojunction device, confirming that TiO_x possesses the right energy level to act efficiently as the ETL in combination with several active blends. Finally, they demonstrated that the properties of the deposited TiO_x remain the same when the deposition process occurs both in air and in a glove box, which is important for the possible implementation of their deposition process into roll-to-roll manufacturing.

Inverted devices that utilize amorphous or crystalline TiO_x (usually deposited by the sol-gel method [29]) are characterized by the same range of efficiencies seen in the case of the ZnO [29,66,67].

The performances of devices incorporating an amorphous TiO_x layer can be boosted with proper tuning of the layer's physical and chemical properties. Choulis and co-workers [68] demonstrated that the PCE of inverted devices can be improved once an ultra-thin layer of polyoxyethylene tridecyl ether (PTE) is inserted as the interlayer between the ITO substrate and the TiO_x layer, a mechanism that apparently resembles the improved electron collection in standard devices when an ultra-thin LiF layer is inserted between the active layer and the top aluminum electrode. They showed no variation in the V_{oc} between samples with and without the PTE interlayer, thus suggesting that no recombination or

morphological behavior differences should characterize the devices. An increase in the J_{sc} was also indicative of reduced leakage current and series resistance. In order to explain such a result, they take into consideration the possible variation of the hydrophilicity of the TiO_x surface, due to the PTE interlayer underneath. Indeed, they found that the TiO_x layer becomes actually more hydrophilic when coated on top of the PTE layer, instead of directly on top of the ITO substrate, thus enhancing the vertical phase separation of the active blend with more of the fullerene phase (relatively more hydrophilic than P3HT [69]) on the bottom and, hence, the electron transport and collection [26,70]. Their results demonstrate how it is possible to clearly improve the PCE of ISCs simply by adding a suitable interlayer on top of the ITO electrode.

They also demonstrated that, even when processed in air, the TiO_x layer can be unaffected by the so-called "light-soaking effect" [71,72]. This is an unusual "s-shaped" current-voltage curve, translating into an extremely low FF, due to the properties of the ITO/TiO_x interface [73], which sometimes arises for air-processed layers. This effect, however, can be suppressed once the TiO_x layer is exposed to UV light, as shown by Kim *et al.* [73]. They proposed a possible mechanism that is responsible for this process: the work function of the TiO_x slightly changes upon UV irradiation, due to the increase of its charge carrier (electrons) density following the suppression of O_2^- traps (adsorbed by TiO_x during realization processes in air), filled with the holes generated by the absorption of the UV radiation. This change in the work function (increased electron density) induces a rearrangement of the Fermi level at the interface (the decreased energy barrier between ITO and TiO_x, see Figure 6) in a direction favorable to a boost in charge transport and collection, resulting in a strong decrease of the series resistance of the device and improved J_{sc}. This mechanism has been exploited to explain also the same findings upon UV irradiation of ZnO layers [59].

Figure 6. The energy diagram of the indium tin oxide (ITO)/TiO_x interface before (**a**) and after (**b**) UV irradiation. Reprinted with permission from [73].

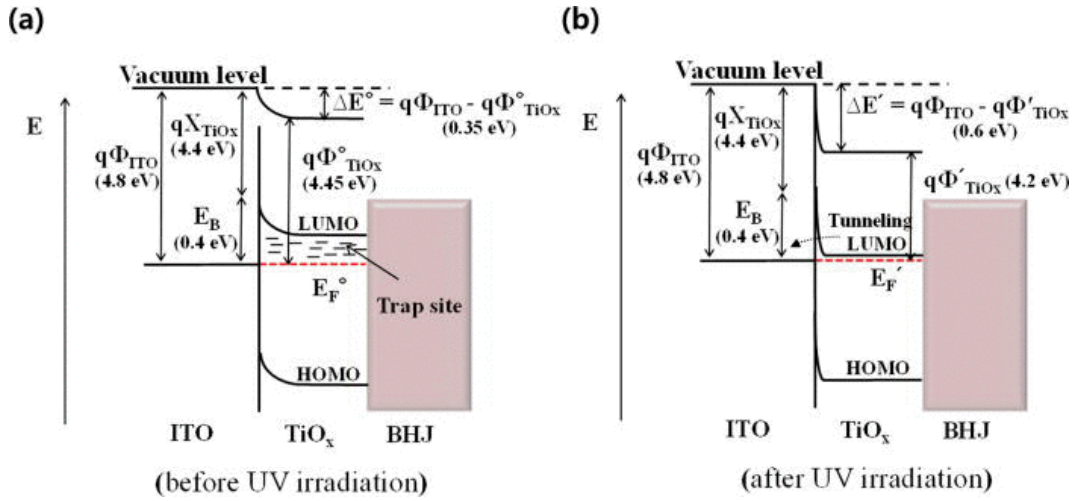

Another elegant way to improve the charge transport and collection and to reduce the charge recombination is by enhancing the vertical phase separation by realizing self-assembled fullerene monolayers (SAM) on top of the TiO_x film [67,74]. Although this seems to be a very good strategy, it is necessary to be careful in the choice of the SAMs: in fact, the deposited layer must resist

the subsequent active layer deposition process from solution, which means that the layer should not present at the end of the process localized defects due to the desorption of molecules [75]. Hsu and coworkers [67] joined together the concepts of self-assembling structures and cross-linking, which were separately exploited previously [76–79], in order to overcome the cited drawback of SAMs, synthesizing a new fullerene-derivative, namely the bis(2-(trichlorosilyl)propyl)malonate C60 (TSMC). This new compound was able to both cross-link and self-assemble on top of the TiO_x layer, without the need for annealing or UV irradiation. The modified TiO_x layer was used in ISCs based on both $PC_{61}BM$ and $PC_{71}BM$, showing a clear improvement of the device parameters, which was explained also by an enhanced vertical phase separation of the active blend by the SAM. Their approach seems to be quite interesting in the framework of facile and practical processes for mass production. Quite in parallel, Kim and coworkers [74] synthesized another fullerene derivative able to generate fullerene-based self-assembled monolayers (FSAMs) onto TiO_x to be used as ETL in ISCs, namely bis-4-(2-ethylhexyloxy)-[6,6]-phenyl C61 butyric acid (bis-p-EHO-PCBA). They showed that the bis-FSAM was responsible for the sensible reduction of the series resistance compared to that of the TiO_x layer alone, with an increase both in J_{sc} and FF in polymer:fullerene-based ISC. This confirms the better wetting properties with the organic active layer (responsible, at the end, for the better device performances) when the TiO_x layer is covered with fullerene-based SAMs.

3.1.3. Cs_2CO_3

The use of Cs_2CO_3 as the ETL is more recent: in 2004, a report from the Canon group [80] described its use in organic light emitting diodes. In 2006, Yang *et al.* [30] showed that such a material could be conveniently used as the ETL in BHJ ISCs: a P3HT:PCBM-based ISC exhibited a good PCE of 2.25% using Cs_2CO_3 in combination with V_2O_5 as the HTL. The interesting result they showed lies in the fact that all the device parameters remained almost unchanged when the Cs_2CO_3 layer was realized by thermal evaporation or by spin coating from solution. They proved that the ETL provided an ohmic contact favorable to the device performance. Liao *et al.* [81] showed that the work function of Cs_2CO_3 can be tuned by annealing the layer at relatively low temperatures up to 200 °C. This shift in the work function is mainly dependent on the intrinsic properties of the layer more than on some chemical reaction with the underlying ITO layer. They also showed a direct correlation between the annealing temperature and both the device PCE and the Cs_2CO_3 surface contact angle, indicating a transition of the ETL from a more hydrophilic-type to a more hydrophobic-type layer, which is beneficial for the subsequent good deposition of the active polymer blend. They explained this work function shift by analyzing the results of XPS experiment, concluding that upon annealing, the Cs_2CO_3 decomposes into Cs_2O oxide doped with Cs_2O_2, thus lowering the WF, with a better matching with the acceptor LUMO and, consequently, the interface resistance.

Xin *et al.* [82] reported on the effect of UV-ozone treatment of Cs_2CO_3 layers on the general performance of BHJ ISCs. They showed that the V_{oc} monotonously decreased with increasing UV-ozone treatment time, while the J_{sc} showed first an increase and then a decrease. The best device performance they obtained was thus attributed to the enhancement of carrier transport and collection by the Cs_2CO_3 layer [83,84]. However, while the effects of UV treatment on ZnO or TiOx layers have been widely studied, the precise mechanism underlying the UV-ozone treatment on the Cs_2CO_3 layer is still unclear.

Other really interesting and recent results were reported by Barbot and coworkers [83]: they exploited the good ETL properties of both Cs_2CO_3 and fullerenes, realizing a Cs_2CO_3-doped C60 ETL interlayer. In a previous work, they found that the electrical conductivity of undoped C60 was improved by eight orders of magnitude upon doping with Cs_2CO_3 for a molar ratio of 1:0.35 [85]. Indeed, they showed that the best BHJ ISC based on a P3HT:PCBM active blend was exactly the one that incorporated an ETL with such a molar concentration ratio, with an increase of V_{oc} and a decrease of the series resistance.

Finally, Liu *et al.* [86] addressed one drawback of the Cs_2CO_3, that is its poor hole blocking ability. By incorporating graphene quantum dots (GQDs) into the Cs_2CO_3, they were able to improve the PCE of a BHJ ISC based on P3HT:PCBM from 2.57% for a reference device with a Cs_2CO_3 ETL only to 3.17% for a device with a GQDs-Cs_2CO_3 ETL. Furthermore, in this case, the better performance was correlated with a better match between the involved energy levels of the ETL and the PCBM, due to a shift of the ETL work function upon incorporation of the GQDs. This minimizes the energy losses at the interface almost without affecting the overall light absorption in the active blend. Moreover, they proposed that an additional exciton dissociation channel could occur at the P3HT/GQD-Cs_2CO_3 interface, facilitating the charge separation. However this could also mean that using such an ETL would affect the vertical phase separation in the active blend, with a non-negligible P3HT phase content on the bottom side of the device that could enhance the charge recombination; this is actually a point that would need to be addressed.

3.1.4. Nb_2O_5

Nb_2O_5 has been used as the ETL in ISCs [87]. A drawback of this metal oxide is that the energy level of its conduction band (about 3.7 eV [88]) is higher than the LUMO level of PCBM (about 3.8 eV [89]); thus, it should not perform as well as ETL in fullerene-based devices. Nevertheless, Cao *et al.* [87] showed that a PCE comparable to that obtained on a similar device, but incorporating a TiO_2 layer as the ETL, is achievable (2.7% compared to 2.8%). They explained this counterintuitive effect with an efficient tunneling process from the PCBM LUMO to the Nb_2O_5 conduction band. Especially when using this metal oxide, great care should be taken in obtaining the optimal layer thickness: a non-optimized layer thickness can even reduce the device PCE close to 0% [87].

3.1.5. Novel Alternatives

Although some of the previous materials dominate the field of electron transport layers in inverted bulk heterojunction solar cells, the surfaces of metal oxides possess hydroxyl groups that are the cause of possible charge trapping [24]. Thus, new materials and concepts have been recently developed as promising alternatives. In particular, towards the development of an all-organic device, the use of polymeric material as ETLs seems to be quite interesting. Huang and coworkers [32] synthesized an amino-functionalized conjugated metallopolymer, namely PFEN-Hg, to be used as an efficient electron transport layer in inverted polymer solar cells. Their polymer was characterized by most of the requirements of an ETL, which are orthogonal solvent processability, transparency to visible light, good electron transport and hole blocking properties, good morphology and effective ITO work function

tuning. With the incorporation of such an ETL, they were able to reach about 9% PCE on an ISC based on PTB7:$PC_{71}BM$ as the active material.

Vijila and coworkers [31] used as the ETL in a P3HT:PCBM-based ISC a solution processable cationic biopolymer, poly(2-(dimethylamino)ethyl methacrylate) (PDMAEMA). They compared the device performance with that of a reference device using a standard ZnO ETL layer, finding comparable PCE for a fresh device and a better stability of the polymeric ETL after eight weeks, with a PCE greater than that of the reference device.

Fang *et al.* [90] developed an ETL based on the hybrid material, CdS/2,9-dimethyl-4,7-diphenyl-1,10- phenanthroline (CdS-BCP), which also fulfills most of the cited requirements for good ETLs. They exploited it in PTB7:$PC_{71}BM$- or P3HT:$PC_{60}BM$-based ISCs, showing an improvement in PCE compared to single CdS or BCP-based devices, with improved stability over time.

Jeon and coworkers [91] took advantage of the good electron transport properties of carbon nanotubes (CNTs) by improving their charge selectivity, coating them with an ultra-thin TiO_x layer deposited by atomic layer deposition. The TiO_x coating, due to its good hole-blocking properties, prevents the recombination of holes and electrons at the metallic part of the CNTs during the charge transport-collection process. This results in a final PCE improvement of about 30% compared to the bare CNTs-based ETL. Although being interesting results, the effectiveness of the TiO_x-coated CNTs strongly depends on the quality (homogeneity and thickness) of the coating, which, if not optimized, can lead to a large amount of leakage current, due to the coating defects.

Kohlstadt *et al.* [92] demonstrated good PCE in ITO-free PTB7:$PC_{71}BM$-based ISC when a metal-metal oxide multilayer is used as the electrode/ETL. They realized by DC magnetron sputtering a sequence of 25 nm of Al-doped ZnO (AZO), 9 nm of silver and, again, 20 nm of AZO. With such a sequential structure, they demonstrated a PCE of 6.1%, almost comparable with the PCE of a standard geometry device with an ITO/PEDOT:PSS substrate (which was reported to be 6.9%). They pointed out that the possible drawback of such a multilayered structure is an unfavorable field distribution inside the active layer and a lower absorption, issues that still need to be addressed.

Oo *et al.* [93] described a very good ETL, namely a zinc tin oxide (ZTO) layer used on top of FTO in P3HT:PCBM-based ISCs. They explained the better performance of the device incorporating the ZTO layer considering the reduced recombination at the interface, the improved electron transport and the hole blocking properties of the ZTO compared to standard ETL.

3.1.6. ETL: Conclusions

As a brief and overall general conclusion on this section, it appears quite clear that optimized (and possibly doped) ZnO and TiOx represent, to date, the best bet for realizing well performing BHJ ISCs, based on the reported averaged PCE of devices and on their fulfillment of most of the points in the "decalogue" established by Litzov and Brabec [29]. Cs_2CO_3, despite its excellent electron transport properties, suffers from poor hole blocking properties [86], while Nb_2O_5 possesses a probably unfavorable energy level diagram to be used generically as the ETL with systems that are not based on PCBM. The other novel alternatives seem really interesting and promising, especially the polymeric ETLs to be fully exploited in the framework of an all-polymer device realized by the roll-to-roll

technique, but the results are too recent in order to be reasonably able to infer some general conclusion over the near future.

3.2. Top Electrode: Hole Collection

In BHJ ISCs, the top metal electrode is usually either gold or silver, due to their intrinsic stability in air. However, Ag is the most suitable top electrode, since its slow oxidation shifts its work function from about 4.3 eV to about 5 eV [94], favoring hole extraction. It has no absorption in the visible range contrary to the evaporated Au layer (slight absorption in the visible) and a higher reflectivity [95]. In fact, Chen *et al*. [96] showed that, *ceteris paribus*, a device with an Ag top metal electrode performed better compared to Au or Al. This is also due to the better matching of the WF of Au (5.1 eV [97]) and the oxidized Ag (around 5.0 eV [94]) with the HOMO levels of the commonly used polymer donors, compared to Al (4.28 eV [97]).

Anyway, in order to obtain good performances from an ISC, the introduction of an HTL layer between the organic active layer and the top metal electrode is mandatory; otherwise, the device would show very poor performance or even no operation at all [98]. To date, the most commonly used HTLs in BHJ ISCs are polymers, like PEDOT:PSS, or metal oxides, like MoO_3, V_2O_5, WO_3, NiO.

3.2.1. PEDOT:PSS

PEDOT:PSS is the most widely used HTL in standard geometry BHJ solar cells, due to its high work function (matching the HOMO level of commonly used donor polymers well), high transparency in the visible range (higher than 80%), good electrical conductivity and the ability to reduce the ITO surface roughness [99], while increasing its work function. However, PEDOT:PSS is highly hydrophilic; thus, bad film morphology and worse electrical properties have been observed when deposited as the HTL onto the hydrophobic organic layers in inverted devices [100,101]. Nevertheless, it is widely used in BHJ ISCs despite this evident drawback. In order to address the wettability problem on hydrophobic surfaces, several strategies have been reported. First of all, the hydrophilic nature of PEDOT:PSS can be reduced by adding proper additives to the polymer dispersion, like isopropyl alcohol [102], or surfactants, like Zonyl FS-300 [103] and Triton X-100 [104], as well as surfactant mixtures [68]. Moon *et al*. [105] added two amphiphilic surfactants, namely Sulfynol 104 EG or PA (dissolved in ethylene glycol or isopropyl alcohol respectively), showing a clear improvement of the PEDOT:PSS layer morphology. This was reflected in an improved P3HT:PCBM-based device performance of about 60% compared to a reference device incorporating the PEDOT:PSS layer without surfactants. The improvement was mainly due to a higher J_{sc} and a higher FF. Indeed, they showed that upon adding the surfactant, the contact angle between the PEDOT:PSS and the underlying organic layer was decreased from 104° to about 53°. This means a clearly better film forming property, resulting in higher shunt resistance (less charge recombination at the electrode) and a lower series resistance (better charge extraction). They explained the better wettability of the additive-added PEDOT:PSS on the organic layer, observing that the used surfactants consist of a hydrophobic alkyl backbone and a hydrophilic hydroxyl group; thus, a van der Waals-type interaction between the hydrophobic alkyl backbone and the hydrophobic P3HT:PCBM surface occurs, making the organic layer hydrophilic with subsequent good PEDOT:PSS

film forming properties on top. Ho and coworkers [106] proposed a novel fluorosurfactants to be used as a substitute to the Zonyl FS-300, since the latter usually needs to be used together with isopropyl alcohol in order to get the best results. The proposed Capstone Dupont FS-31 can be used alone as an additive to the PEDOT:PSS, giving very good results in terms of overall device performance when a relative concentration of about 5% is used. They also showed that the additive concentration in the PEDOT:PSS dispersion greatly affects the final film forming, thus reflecting in better or worse device performances. A concentration below 4% results in a non-uniform layer, due to the still low wettability onto the organic layer. On the contrary, if the concentration is too high (above 8%), the presence of excess surfactant reduces the charge conduction pathway through the PEDOT molecules, thus resulting in poor charge collection. Moreover, they showed that the surfactant also promotes a phase segregation between PEDOT and PSS, thus resulting in a well-formed PEDOT conduction pathway, while favoring a good physical contact with the underlying organic layer.

Another strategy to improve the PEDOT:PSS adhesion onto the organic layer is to exploit different deposition techniques rather than spin coating. Gupta and coworkers [107] obtained efficient P3HT:PCBM-based inverted OSCs by realizing the top PEDOT:PSS contact by stamp-transfer lamination. They showed that this process does not induce significant losses on the open circuit voltage, nor does it increase the overall resistance of the devices.

However, despite the progresses towards a better adhesion of PEDOT:PSS on top of organic layers, the acidic/hygroscopic nature of the compound is still detrimental for the top-side metal electrode. Indeed, Kim and coworkers clearly showed [108] that PEDOT:PSS is able to promote the corrosion and degradation of a thin layer of Ag as typically used in ISCs. They demonstrated that the hygroscopic nature of PEDOT:PSS promotes a very fast absorption of ambient water inside the layer. This absorbed water becomes corrosive, due to the acidic nature of the PEDOT:PSS, thus slowly corroding the silver layer, first promoting grain boundary grooves, then leading to grain segregation, forming separated particles. They, however, observed that such a process could be slow in a real device configuration and processing, although in the long term, it would cause strong degradation of the performances.

Even if, to date, PEDOT:PSS is still the most used HTL in inverted BHJ PSCs [29], in order to avoid all these drawbacks, in several works, PEDOT:PSS has been replaced by other efficient HTLs, like the following ones.

3.2.2. MoO_3

A thin HTL of molybdenum trioxide (MoO_3) greatly improves the performance of both inverted and conventional OLEDs [109–111]. Early in 2008, Chen and coworkers [96] showed that MoO_3 increased the overall efficiency of a BHJ ISC based on both a P3HT:PCBM active layer and a nanocrystalline TiO_2 ETL. They reported that the V_{oc} of the device changed only slightly when the top metal electrode was varied from Ag to Au to Al, while the optimal HTL thickness depends on the chosen metal. In particular, with Al as top electrode, an higher thickness of the evaporated MoO_3 layer is required in order to obtain the same performances of devices using Ag or Au. This was attributed to the chemical reaction between Al and MoO_3 during the evaporation process, forming a MoO_2 species, due to the reduction of MoO_3.

The dependence of the overall efficiency of devices on the MoO_3 thickness has been also detailed by Zheng *et al.* [112] and by Wantz and coworkers [113]. Zheng *et al.* showed that the PIFTBT8:$PC_{71}BM$-

based device parameters remained almost unchanged when the thickness of the MoO_3 layer was in the range of 10–20 nm, while a drop in both V_{oc} and FF occurred when the thickness was decreased to 5 nm. They correlated such a behavior with the shunt and the series resistance, observing that a decrease of the thickness of the MoO_3 layer was followed by both an increase of the series resistance and a decrease of the shunt resistance. Moreover, increasing the thickness, the V_{oc} changed from 1.00 V to 1.04 V, and the FF varied between 41.9% and 50%. Wantz *et al.* showed that the overall performance of a P3HT:PCBM-based device was only slightly affected by a variation of the MoO_3 thickness from 6 nm to 22 nm. Interestingly, they also demonstrated how the post-processing thermal treatment on the device, usually employed to improve the device performance [114], is, on the contrary, detrimental in BHJ ISCs when MoO_3 is used as the HTL. In fact, they observed that after 10 min at 170 °C, the cohesion between the MoO_3 layer and the silver electrode was lost, and the layer itself evolved into an alloy of silver and molybdenum oxide, with a diffusion of silver ions and oxygen inside the active layer. The thinner the MoO_3 layer, the faster and even worse was this process. It should then be concluded that an inverted BHJ incorporating an MoO_3 layer should not undergo a thermal treatment after the completion of the device. However, since in the case of P3HT:PCBM, the annealing process promotes the vertical phase separation in a way favorable to the inverted device working principle [115], such an annealing process should be performed *prior* to the deposition of both the HTL and the top metal electrode. Moreover, providing that the post-processing annealing treatment is avoided for the completed device, Gupta and coworkers [116] showed that MoO_3 acts as a barrier to the diffusion of metal ions and oxygen inside the active layer, thus preventing fast device degradation. The role of the environment on the effects of the thermal treatment of thin layers of MoO_3 was studied by Vijila and coworkers [117]. When the complete device incorporating the MoO_3 layer as the HTL is annealed in vacuum, the overall stability and performance are higher compared to a similar device annealed in a nitrogen atmosphere. The difference in the PCE was increased upon aging, with the vacuum annealed device retaining 80% of its initial PCE value after 30 days compared to the 50% of the device annealed in nitrogen atmosphere. They explained this behavior observing that the metal oxide layer annealed in vacuum is characterized by an oxygen deficient structure that is the origin of an enhanced hole-conducting properties.

Jiang *et al.* [118] demonstrated that an interesting way to improve and tune the electrical and the optical properties of a MoO_3 layer can be by realizing a composite film with Au. They showed that a MoO_3-Au (30%) layer is characterized by very good electrical and optical parameters. They exploited this layer as the HTL in a conventional geometry solar cell, in substitution of PEDOT:PSS. Although there is no report on the use of such a modified MoO_3 layer in inverted devices, one can speculate that such a layer could be conveniently exploited also in this type of solar cell.

3.2.3. WO_3

As shown earlier by Dong *et al.* [97], the high work function of WO_3 (-4.8 eV) greatly enhances the hole transport and collection at the WO_3/Ag interface. They showed that the optimum thickness for WO_3 in a P3HT:PCBM-based device is in the range between five and 10 nm. Lower values would results in poor coverage of the film, while higher values would increase the series resistance, thus lowering the overall device performance. They also showed that the V_{oc} of the devices were substantially unaffected by the choice of the top metal electrode (Au, Ag or Al). Kwon *et al.* [119] compared the performances

of MoO_3 and WO_3 inverted devices based on several active layers. They showed that in all cases, the device incorporating a WO_3 HTL layer (5 nm optimum thickness) performed slightly better than those with a MoO_3 HTL layer (10 nm optimum thickness). They explained this better behavior of the WO_3 layer with: (1) a better film surface morphology (a reduced average roughness measured by atomic force microscopy); (2) a better measured conductivity; and (3) better electron blocking and hole transport properties, due to the higher energy barrier between the donor LUMO and the HTL conduction band and the better matching between the donor HOMO level and valence band of the HTL.

Brabec *et al.* [120] demonstrated that a low temperature (80 °C) solution-processed nanoparticle WO_3 HTL was able to perform as well as PEDOT:PSS in a standard geometry device and to give very good performances on an inverted architecture. The solution was alcohol-based and free of any surfactant, and the realized HTL does not need any oxygen-plasma treatment, which is usually required to remove the dispersing agent in the original NP dispersion [121] and to improve its HTL properties. They concluded that the low temperature solution-processed WO_3 layer can be easily and conveniently exploited in flexible solar cell production processes.

3.2.4. V_2O_5 and NiO

Even if V_2O_5 has been used as the HTL in inverted devices,-its high toxicity [119] makes it not very suitable for easy and low cost device processing in ambient conditions. Moreover Riedl *et al.* [121] showed that care should be taken when realizing the V_2O_5 HTL by the sol-gel process. They compared the performance of P3HT:PCBM-based devices with evaporated V_2O_5 HTL or sol-gel-processed V_2O_5 HTL, observing that the 10 nm-thick layer of the sol-gel-processed V_2O_5 sensibly affects the working device, depending on the initial solution concentration and spin coating speed. In particular, a low concentration of the precursor solution (1:150) spin coated at slow speed formed a film that affected the device positively, showing parameters comparable to those obtained with an evaporated V_2O_5 layer. On the contrary, a film with the same thickness, but obtained from a higher concentrated precursor solution (1:70), spin coated at a higher speed, greatly lowered the overall performance of the device. They excluded that such a strange behavior could be attributed to some effect of the solvent onto the active layer, while showing through XPS measurements that the higher concentrated precursor solution leads to a deep penetration of vanadium inside the active layer, up to more than 100 nm. This penetration of the precursor into the active layer (that was by far less evident in the case of the evaporated V_2O_5) could damage the P3HT chains and/or lead to the quenching of excitons in the donor phase. This penetration was also indirectly confirmed by Dauskardt and coworkers [115] when comparing the roll-to-roll-processed inverted BHJ PSC incorporating both PEDOT:PSS or V_2O_5 HTLs.

NiO has been also used as a good HTL in BHJ ISC. NiO possesses a valence band and a conduction band at -5.0 eV and -1.7 eV, respectively, thus acting as a good HTL and a good electron blocking layer in combination with a P3HT:PCBM, as shown by Chen and coworkers [122]. The optimal HTL thickness in their case was under 2 nm, above which the device performance starts to decrease. They attributed this behavior to the intrinsic electronic properties of the NiO layer that was deposited in a high vacuum by thermal evaporation, thus affecting the oxygen concentration in the realized layer. A thin layer was also deposited from solution by Lee *et al.* [123], by simply dissolving NiO powder into various solvents (the best was found to be isopropyl alcohol) and spin coating it onto the P3HT:PCBM active layer. Upon

optimization of the active layer thickness, they were able to obtain about 3% PCE, comparable with a reference device incorporating as the HTL a thin layer of PEDOT:PSS. The solution processable NiO layer could be compatible with roll-to-roll manufacturing in air.

3.2.5. Novel Alternatives

A solution processable mixture of V_2O_5 and MoO_3 was exploited by Huang and coworkers [124] as an efficient HTL in a P3HT:PCBM-based inverted solar cell. They showed that the mixed layer causes a significant improvement of the device parameters compared to control devices with V_2O_5 or WO_3 HTL alone. They explained these results with the efficient hole transport, due to the well matched donor HOMO-valence band of V_2O_5 and, concomitantly, to the electron extraction from the top silver electrode through the conduction band of the WO_3. This complementary mechanism positively affects the overall device PCE.

Solution-processable triindoles, namely triazatruxene (TAT) and N-trimethyltriindole (TMTI), with tailored HOMO and LUMO levels, in order to be used as the HTL in inverted devices, were presented by Ma *et al*. [125]. They showed an improvement in the J_{sc} and in the overall PCE of a P3HT:PCBM-based inverted device when a thin layer of TAT was spin coated onto the active layer.

Furthermore, graphene oxide has been exploited as the HTL in BHJ PSCs by Dai and coworker [126]. Indeed, graphene is a bidimensional carbon structure that possesses excellent electronic and mechanical properties [127]. Through the neutralization of the –COOH groups of the graphene oxide with Cs_2CO_3, they were able to tune the electronic properties of the material, giving both excellent ETL or HTL properties. They exploited these interesting characteristics, showing very good device performances in P3HT:PCBM-based devices with a PCE exceeding 3%.

A 4.4% PCE on a P3HT:PCBM device was achieved by Chen *et al*. [128] by developing a self-assembled HTL strategy. They synthesized a novel fluoroalkyl side-chain diblock copolymer, namely the poly(3-hexylthiophene)-block-poly[3-(4-(3,3,4,4,5,5,6,6,7,7,8,8,8-tridecafluorooctyloxy)phenyl)-decyloxy)thiophene] (P3HT-b-P3FAT), in which, upon spin coating, the fluorinated moiety spontaneously undergoes a segregation on top of the P3HT phase, due to the low surface energy of the fluoroalkyl chains, forming a self-assembled HTL. Exploiting this mechanism and controlling the block ratio into the copolymer, they were able to greatly improve the hole collection and, thus, the overall efficiency of the device.

3.2.6. HTLs: Conclusions

Averaging the general results, it should be concluded that the best HTL for BHJ ISCs should be a thin layer of either MoO_3 or WO_3, due to their intrinsic good electrical and optical properties, their ability to prevent oxygen and metal ion diffusion into the active layer and the almost unchanged device parameters upon slight variation of their optimum thickness. On the contrary, PEDOT:PSS has to be avoided, due to its evident drawbacks, as mentioned. Dauskardt and coworkers [115] demonstrated how the poor adhesion of PEDOT:PSS onto the active layer results in a general loss of device performance in a roll-to-roll processed device, due to the thermomechanical stress that every "real-life" device would undergo.

However, it appears clear (see, for example, the comparison between MoO_3 and WO_3 above) that the key factor in choosing the best HTL is the trade-off between the electrical/morphological properties and the energetics involved at the interfaces in the particular device. This means that for each particular donor-acceptor system, the matching between the HOMO and LUMO levels of the organic phases and the valence band and the conduction band of the HTL should be optimum. Not only the HOMO level of the donor should match with the valence band of the HTL, but also the latter should have a conduction band far from the active layers' LUMO level, otherwise resulting in an enhanced charge recombination and poor electron blocking behavior [112]. Finally, when dealing with metal-oxides, it should be also considered (in the proper choosing of the best HTL for the particular system) that the work function of those materials strongly depends on the concentration of defects [129], with a decrease of the WF if oxygen is removed from the material, and an increase in the WF is observed with oxygen addition. Interestingly, Xie and Choy [130] developed a synthesis route for developing low-temperature solution-processed MoO_3 or V_2O_5 HTL with the ability to control the oxygen vacancies, thus, in the end, controlling the final WF.

Finally, one key motivation in selecting the proper HTL should be the compatibility of its deposition process with standard roll-to-roll or printing techniques for the realization of complete devices in ambient conditions, without the need for vacuum processes, like thermal evaporation. Thus, the choice should come down to solution processable HTLs, which is no longer a limitation, since solution-processed WO_3 and MoO_3 HTLs have been exploited both in conventional and inverted devices, showing good overall performances [120,131–134]. Furthermore, the very interesting polymeric novel alternatives cited above could be promising.

4. Device Stability: A Brief Comment

Considering the environmental stability in the working condition of a BHJ ISC as the *key* parameter, which is the best ETL and HTL choice? Actually it is not possible, to date, to give a precise answer. A detailed discussion on this issue is far beyond the scope of this paper: in one sentence, the stability of BHJ ISCs is still a matter of debate [29]. For example, it is not clear how and to what extent the particular process used for preparing metal oxide layers can affect the final device stability [135], nor which is the particular "best" device structure [136]. One comprehensive study on the stability of several ETL/HTL combinations has recently been performed by Voroshazi and coworkers [137]. They demonstrated that ZnO- and TiO_x-based devices were comparably stable in air for over 1000 h, while the analyzed organic ETLs were clearly affected by a lower stability over time. On the HTL side, they surprisingly showed that a PEDOT:PSS-based device was more stable than a MoO_3-based device. However, Vijila and coworkers [117] demonstrated that the annealing condition of a MoO3-based device can greatly affect the final device stability. They demonstrated that a vacuum annealed device was characterized by a 10% increased stability compared to a device annealed in a nitrogen atmosphere, as discussed in the previous section. Furthermore, Sun *et al.* [38] showed that a device incorporating a thin layer of MoO_3 as the HTL retained 70% of its initial PCE after 30 days.

Finally, some recent reports on lifecycle analysis (LCA) and energy payback time (EPT) have been published by several groups [138–140]. From the reported results, it can be concluded that it is

quite difficult to assess a precise standard, to date, in order to definitively compare different kinds of devices, materials and procedures. Even the same devices are characterized by some variation in their working parameters when measured by different laboratories [136]. A definition of a precise standard in this field should be particularly important to evaluate how much the (sometimes low) increase in the PCE obtained with a particular process/optimization of the ETLs and/or the HTLs is convenient from an economical point of view (considering the energy and time consumption needed for the layer realization/optimization).

5. General Conclusions

As a general conclusion, the BHJ ISC appears to be a very promising device structure to be exploited in the mass production of organic solar cells. Aside from the development and optimization of novel active materials, like novel acceptors or low band-gap polymer donors, the correct optimization and choice of the HTL together with the ETL play a fundamental role in order to get the best performance from a device. Many parameters, however, need to be traded off, as has been described. In particular, a necessary trade-off between better HTL and ETL electrical properties and overall device optical properties must be accomplished. Moreover, the right HTL, as well as the right ETL must be chosen, taking into account the energy level structure of the particular active blend used. The ideal optimum is the matching between the donor HOMO and the valence band of the HTL and between the acceptor LUMO and the conduction band of the ETL, together with a proper position of the HTL conduction band and the ETL valence band, in order to provide, at the same time, a good electron blocking or hole blocking behavior, respectively. The same features are also relevant in the case of polymeric or organic HTLs and ETLs (in this case, the matching should be between the HOMO and LUMO levels of the active layer and the HOMO and LUMO levels of the other layers).

As has been pointed out in the previous sections, the ETL and HTL performances can be affected by the realization parameters. Good control and knowledge of all these parameters should be necessary in order to get the maximum performance from a given system.

As a final remark, it is important to stress that novel polymeric alternatives could come in handy for bypassing the depicted criticality typical of the most used metal oxides, being also intrinsically compatible with low-cost device manufacturing processes.

Acknowledgments

Marco Anni is gratefully acknowledged for useful comments and suggestions.

Conflicts of Interest

The author declares no conflicts of interest.

References

1. Shirakawa, H.; Louis, E.J.; MacDiarmid, A.G.; Chiang, C.K.; Heeger, A.J. Synthesis of electrically conducting organic polymers: Halogen derivatives of polyacetylene, (CH)x. *J. Chem. Soc. Chem. Commun.* **1977**, 578–580, doi:10.1039/C39770000578.
2. Service, R.F. Outlook brightens for plastic solar cells. *Science* **2011**, *332*, 293.
3. Scharber, M.; Sariciftci, N.S. Efficiency of bulk-heterojunction organic solar cells. *Prog. Polym. Sci.* **2013**, *38*, 1929–1940.
4. Jorgensen, M.; Carlé, J.E.; Sondergaard, R.R.; Lauritzen, M.; Dagnaes-Hansen, N.A.; Byskov, S.L.; Andersen, T.R.; Larsen-Olsen, T.T.; Böttiger, A.P.; Andreasen, B.; *et al*. The state of organic solar cells—A meta analysis. *Sol. Energy Mater. Sol. Cells* **2013**, *119*, 84–93.
5. Tang, C.W. Two-layer organic photovoltaic cell. *Appl. Phys. Lett.* **1986**, *48*, 183–185.
6. Sariciftci, N.; Smilowitz, L.; Heeger, A.; Wudl, F. Semiconducting polymers (as donors) and buckminsterfullerene (as acceptor): Photoinduced electron transfer and heterojunction devices. *Synth. Met.* **1993**, *59*, 333–352.
7. Sariciftci, N.S.; Braun, D.; Zhang, C.; Srdanov, V.I.; Heeger, A.J.; Stucky, G.; Wudl, F. Semiconducting polymer-buckminsterfullerene heterojunctions: Diodes, photodiodes, and photovoltaic cells. *Appl. Phys. Lett.* **1993**, *62*, 585–587.
8. Yu, G.; Pakbaz, K.; Heeger, A.J. Semiconducting polymer diodes: Large size, low cost photodetectors with excellent visible-ultraviolet sensitivity. *Appl. Phys. Lett.* **1994**, *64*, 3422–3424.
9. Hummelen, J.C.; Knight, B.W.; LePeq, F.; Wudl, F.; Yao, J.; Wilkins, C.L. Preparation and characterization of fulleroid and methanofullerene derivatives. *J. Org. Chem.* **1995**, *60*, 532–538.
10. Yu, G.; Gao, J.; Hummelen, J.C.; Wudl, F.; Heeger, A.J. Polymer photovoltaic cells: Enhanced efficiencies via a network of internal donor-acceptor heterojunctions. *Science* **1995**, *270*, 1789–1791.
11. Tremolet de Villers, B.; Tassone, C.J.; Tolbert, S.H.; Schwartz, B.J. Improving the reproducibility of P3HT:PCBM solar cells by controlling the PCBM/cathode interface. *J. Phys. Chem. C* **2009**, *113*, 18978–18982.
12. Sanyal, M.; Schmidt-Hansberg, B.; Klein, M.F.G.; Colsmann, A.; Munuera, C.; Vorobiev, A.; Lemmer, U.; Schabel, W.; Dosch, H.; Barrena, E. *In Situ* X-ray study of drying-temperature influence on the structural evolution of bulk-heterojunction polymer-fullerene solar cells processed by doctor-blading. *Adv. Energy Mater.* **2011**, *1*, 363–367.
13. Hoth, C.N.; Choulis, S.A.; Schilinsky, P.; Brabec, C.J. On the effect of poly(3-hexylthiophene) regioregularity on inkjet printed organic solar cells. *J. Mater. Chem.* **2009**, *19*, 5398–5404.
14. Nie, W.; Coffin, R.; Liu, J.; MacNeill, C.M.; Li, Y.; Noftle, R.E.; Carroll, D.L. Exploring spray-coating techniques for organic solar cell applications. *Int. J. Photoenergy* **2012**, *2012*, doi:10.1155/2012/175610.
15. Kim, Y.H.; Lee, S.H.; Noh, J.; Han, S.H. Performance and stability of electroluminescent device with self-assembled layers of poly(3,4-ethylenedioxythiophene)-poly(styrenesulfonate) and polyelectrolytes. *Thin Solid Films* **2006**, *510*, 305–310.

16. De Jong, M.P.; van IJzendoorn, L.J.; de Voigt, M.J.A. Stability of the interface between indium-tin-oxide and poly(3,4-ethylenedioxythiophene)/poly(styrenesulfonate) in polymer light-emitting diodes. *Appl. Phys. Lett.* **2000**, *77*, 2255–2257.
17. Yim, K.H.; Zheng, Z.; Friend, R.H.; Huck, W.T.S.; Kim, J.S. Surface-directed phase separation of conjugated polymer blends for efficient light-emitting diodes. *Adv. Funct. Mater.* **2008**, *18*, 2897–2904.
18. Pavlopoulou, E.; Fleury, G.; Deribew, D.; Cousin, F.; Geoghegan, M.; Hadziioannou, G. Phase separation-driven stratification in conventional and inverted P3HT:PCBM organic solar cells. *Org. Electron.* **2013**, *14*, 1249–1254.
19. Baigent, D.R.; Marks, R.N.; Greenham, N.C.; Friend, R.H.; Moratti, S.C.; Holmes, A.B. Conjugated polymer light-emitting diodes on silicon substrates. *Appl. Phys. Lett.* **1994**, *65*, 2636–2638.
20. Arias, A.C.; Granström, M.; Thomas, D.S.; Petritsch, K.; Friend, R.H. Doped conducting-polymer–semiconducting-polymer interfaces: Their use in organic photovoltaic devices. *Phys. Rev. B* **1999**, *60*, 1854–1860.
21. Nyberg, T. An alternative method to build organic photodiodes. *Synth. Met.* **2004**, *140*, 281–286.
22. Ameri, T.; Dennler, G.; Waldauf, C.; Denk, P.; Forberich, K.; Scharber, M.C.; Brabec, C.J.; Hingerl, K. Realization, characterization, and optical modeling of inverted bulk-heterojunction organic solar cells. *J. Appl. Phys.* **2008**, *103*, 084506.
23. Yuan, J.; Huang, X.; Dong, H.; Lu, J.; Yang, T.; Li, Y.; Gallagher, A.; Ma, W. Structure, band gap and energy level modulations for obtaining efficient materials in inverted polymer solar cells. *Org. Electron.* **2013**, *14*, 635–643.
24. Hau, S.K.; Yip, H.L.; Jen, A.K.Y. A review on the development of the inverted polymer solar cell architecture. *Polym. Rev.* **2010**, *50*, 474–510,
25. Zhang, F.; Xu, X.; Tang, W.; Zhang, J.; Zhuo, Z.; Wang, J.; Wang, J.; Xu, Z.; Wang, Y. Recent development of the inverted configuration organic solar cells. *Sol. Energy Mater. Sol. Cells* **2011**, *95*, 1785–1799.
26. Deibel, C.; Dyakonov, V. Polymer-fullerene bulk heterojunction solar cells. *Rep. Prog. Phys.* **2010**, *73*, 096401.
27. Chen, D.; Zhang, C.; Wang, Z.; Zhang, J.; Feng, Q.; Xu, S.; Zhou, X.; Hao, Y. Performance comparison of conventional and inverted organic bulk heterojunction solar cells from optical and electrical aspects. *IEEE Trans. Electron Devices* **2013**, *60*, 451–457.
28. Murphy, L.; Hong, W.; Aziz, H.; Li, Y. Organic photovoltaics with thick active layers (800 nm) using a high mobility polymer donor. *Sol. Energy Mater. Sol. Cells* **2013**, *114*, 71–81.
29. Litzov, I.; Brabec, C.J. Development of efficient and stable inverted bulk heterojunction (BHJ) solar cells using different metal oxide interfaces. *Materials* **2013**, *6*, 5796–5820.
30. Li, G.; Chu, C.W.; Shrotriya, V.; Huang, J.; Yang, Y. Efficient inverted polymer solar cells. *Appl. Phys. Lett.* **2006**, *88*, 253503.
31. Jin Tan, M.; Zhong, S.; Wang, R.; Zhang, Z.; Vijila, C.; Chen, W. Biopolymer as an electron selective layer for inverted polymer solar cells. *Appl. Phys. Lett.* **2013**, *103*, 063303.

32. Liu, S.; Zhang, K.; Lu, J.; Zhang, J.; Yip, H.L.; Huang, F.; Cao, Y. High-efficiency polymer solar cells via the incorporation of an amino-functionalized conjugated metallopolymer as a cathode interlayer. *J. Am. Chem. Soc.* **2013**, *135*, 15326–15329.
33. Kyaw, A.K.K.; Sun, X.W.; Jiang, C.Y.; Lo, G.Q.; Zhao, D.W.; Kwong, D.L. An inverted organic solar cell employing a sol-gel derived ZnO electron selective layer and thermal evaporated MoO3 hole selective layer. *Appl. Phys. Lett.* **2008**, *93*, 221107.
34. Kang, Y.J.; Lim, K.; Jung, S.; Kim, D.G.; Kim, J.K.; Kim, C.S.; Kim, S.H.; Kang, J.W. Spray-coated ZnO electron transport layer for air-stable inverted organic solar cells. *Sol. Energy Mater. Sol. Cells* **2012**, *96*, 137–140.
35. Ibrahem, M.A.; Wei, H.Y.; Tsai, M.H.; Ho, K.C.; Shyue, J.J.; Chu, C.W. Solution-processed zinc oxide nanoparticles as interlayer materials for inverted organic solar cells. *Sol. Energy Mater. Sol. Cells* **2013**, *108*, 156–163.
36. Mahmood, A.; Ahmed, N.; Raza, Q.; Khan, T.M.; Mehmood, M.; Hassan, M.M.; Mahmood, N. Effect of thermal annealing on the structural and optical properties of ZnO thin films deposited by the reactive e-beam evaporation technique. *Phys. Scr.* **2010**, *82*, 065801.
37. Park, H.Y.; Lim, D.; Kim, K.D.; Jang, S.Y. Performance optimization of low-temperature-annealed solution-processable ZnO buffer layers for inverted polymer solar cells. *J. Mater. Chem. A* **2013**, *1*, 6327–6334.
38. Sun, Y.; Seo, J.H.; Takacs, C.J.; Seifter, J.; Heeger, A.J. Inverted polymer solar cells integrated with a low-temperature-annealed sol-gel-derived ZnO film as an electron transport layer. *Adv. Mater.* **2011**, *23*, 1679–1683.
39. Hu, T.; Li, F.; Yuan, K.; Chen, Y. Efficiency and air-stability improvement of flexible inverted polymer solar cells using ZnO/poly(ethylene glycol) hybrids as cathode buffer layers. *ACS Appl. Mater. Interfaces* **2013**, *5*, 5763–5770.
40. Yu, X.; Yu, X.; Hu, Z.; Zhang, J.; Zhao, G.; Zhao, Y. Effect of sol-gel derived ZnO annealing rate on light-trapping in inverted polymer solar cells. *Mater. Lett.* **2013**, *108*, 50–53.
41. Ohyama, M.; Kouzuka, H.; Yoko, T. Sol-gel preparation of ZnO films with extremely preferred orientation along (002) plane from zinc acetate solution. *Thin Solid Films* **1997**, *306*, 78–85.
42. Hu, Z.; Zhang, J.; Liu, Y.; Hao, Z.; Zhang, X.; Zhao, Y. Influence of ZnO interlayer on the performance of inverted organic photovoltaic device. *Sol. Energy Mater. Sol. Cells* **2011**, *95*, 2126–2130.
43. Dhibi, O.; Ltaief, A.; Zghal, S.; Bouazizi, A. Inverted low band gap polymer solar cells integrated with a low-temperature-annealed sol-gel-derived ZnO: Active layer thickness effect on the recombination process. *Superlattices Microstruct.* **2013**, *60*, 548–560.
44. Nickel, F.; Sprau, C.; Klein, M.F.; Kapetana, P.; Christ, N.; Liu, X.; Klinkhammer, S.; Lemmer, U.; Colsmann, A. Spatial mapping of photocurrents in organic solar cells comprising wedge-shaped absorber layers for an efficient material screening. *Sol. Energy Mater. Sol. Cells* **2012**, *104*, 18–22.
45. Elumalai, N.K.; Vijila, C.; Jose, R.; Zhi Ming, K.; Saha, A.; Ramakrishna, S. Simultaneous improvements in power conversion efficiency and operational stability of polymer solar cells by interfacial engineering. *Phys. Chem. Chem. Phys.* **2013**, *15*, 19057–19064.

46. Hu, Z.; Zhang, J.; Zhu, Y. Inverted polymer solar cells with a boron-doped zinc oxide layer deposited by metal organic chemical vapor deposition. *Sol. Energy Mater. Sol. Cells* **2013**, *117*, 610–616.
47. Park, B.; Shin, J.C.; Huh, Y.H. Interface-engineering additives for inverted {BHJ} polymer solar cells. *Sol. Energy Mater. Sol. Cells* **2013**, *110*, 15–23.
48. Liu, Y.; Larsen-Olsen, T.T.; Zhao, X.; Andreasen, B.; Sondergaard, R.R.; Helgesen, M.; Norrman, K.; Jorgensen, M.; Krebs, F.C.; Zhan, X. All polymer photovoltaics: From small inverted devices to large roll-to-roll coated and printed solar cells. *Sol. Energy Mater. Sol. Cells* **2013**, *112*, 157–162.
49. Alstrup, J.; Jorgensen, M.; Medford, A.J.; Krebs, F.C. Ultra Fast and parsimonious materials screening for polymer solar cells using differentially pumped slot-die coating. *ACS Appl. Mater. Interfaces* **2010**, *2*, 2819–2827.
50. Perulli, A.; Lattante, S.; Persano, A.; Cola, A.; di Giulio, M.; Anni, M. On the spatial inhomogeneity of charge generation and collection in inverted all polymer solar cells. *Appl. Phys. Lett.* **2013**, *103*, 053305.
51. Ajuria, J.; Etxebarria, I.; Azaceta, E.; Tena-Zaera, R.; Fernandez-Montcada, N.; Palomares, E.; Pacios, R. Novel ZnO nanostructured electrodes for higher power conversion efficiencies in polymeric solar cells. *Phys. Chem. Chem. Phys.* **2011**, *13*, 20871–20876.
52. Liang, Z.; Gao, R.; Lan, J.L.; Wiranwetchayan, O.; Zhang, Q.; Li, C.; Cao, G. Growth of vertically aligned ZnO nanowalls for inverted polymer solar cells. *Sol. Energy Mater. Sol. Cells* **2013**, *117*, 34–40.
53. Elumalai, N.K.; Jin, T.M.; Vijila, C.; Jose, R.; Palaniswamy, S.K.; Jayaraman, S.; Raut, H.K.; Ramakrishna, S. Electrospun ZnO nanowire plantations in the electron transport layer for high-efficiency inverted organic solar cells. *ACS Appl. Mater. Interfaces* **2013**, *5*, 9396–9404,
54. Bhat, J.S.; Patil, A.S.; Swami, N.; Mulimani, B.G.; Gayathri, B.R.; Deshpande, N.G.; Kim, G.H.; Seo, M.S.; Lee, Y.P. Electron irradiation effects on electrical and optical properties of sol-gel prepared ZnO films. *J. Appl. Phys.* **2010**, *108*, 043513.
55. Ohyama, M.; Kozuka, H.; Yoko, T. Sol-gel preparation of transparent and conductive aluminum-doped zinc oxide films with highly preferential crystal orientation. *J. Am. Ceram. Soc.* **1998**, *81*, 1622–1632.
56. Lee, S.H.; Kim, J.H.; Shim, T.H.; Park, J.G. Effect of interface thickness on power conversion efficiency of polymer photovoltaic cells. *Electron. Mater. Lett.* **2009**, *5*, 47–50.
57. Lattante, S.; Perulli, A.; Anni, M. Study of the series resistance evolution in organic solar cells by use of the Lambert W function. *Synth. Met.* **2011**, *161*, 949–952.
58. Chang, J.; Lin, Z.; Zhu, C.; Chi, C.; Zhang, J.; Wu, J. Solution-processed LiF-doped ZnO films for high performance low temperature field effect transistors and inverted solar cells. *ACS Appl. Mater. Interfaces* **2013**, *5*, 6687–6693.
59. Du, X.; He, D.; Xiao, Z.; Ding, L. The double-edged function of UV light in polymer solar cells with an inverted structure. *Synth. Met.* **2012**, *162*, 2302–2306.
60. Girolamo, V.B.M.; Antonucci, V.; Aricó, A.S. Influence of TiO2 film thickness on the electrochemical behaviour of dye-sensitized solar cells. *Int. J. Electrochem. Sci.* **2011**, *6*, 3375.

61. Sakohara, S.; Ishida, M.; Anderson, M.A. Visible luminescence and surface properties of nanosized ZnO colloids prepared by hydrolyzing Zinc acetate. *J. Phys. Chem. B* **1998**, *102*, 10169–10175,
62. Monticone, S.; Tufeu, R.; Kanaev, A.V. Complex nature of the UV and visible fluorescence of colloidal ZnO nanoparticles. *J. Phys. Chem. B* **1998**, *102*, 2854–2862.
63. Peng, R.; Yang, F.; Ouyang, X.; Liu, Y.; Kim, Y.S.; Ge, Z. Enhanced photovoltaic performance of inverted polymer solar cells by tuning the structures of titanium dioxide. *Thin Solid Films* **2013**, *545*, 424–428.
64. Kuwabara, T.; Sugiyama, H.; Yamaguchi, T.; Takahashi, K. Inverted type bulk-heterojunction organic solar cell using electrodeposited titanium oxide thin films as electron collector electrode. *Thin Solid Films* **2009**, *517*, 3766–3769.
65. Kim, J.Y.; Kim, S.H.; Lee, H.H.; Lee, K.; Ma, W.; Gong, X.; Heeger, A.J. New architecture for high-efficiency polymer photovoltaic cells using solution-based titanium oxide as an optical spacer. *Adv. Mater.* **2006**, *18*, 572–576.
66. Hadipour, A.; Maller, R.; Heremans, P. Room temperature solution-processed electron transport layer for organic solar cells. *Org. Electron.* **2013**, *14*, 2379–2386.
67. Liang, W.W.; Chang, C.Y.; Lai, Y.Y.; Cheng, S.W.; Chang, H.H.; Lai, Y.Y.; Cheng, Y.J.; Wang, C.L.; Hsu, C.S. Formation of nanostructured fullerene interlayer through accelerated self-assembly and cross-linking of trichlorosilane moieties leading to enhanced efficiency of photovoltaic cells. *Macromolecules* **2013**, *46*, 4781–4789.
68. Savva, A.; Neophytou, M.; Koutsides, C.; Kalli, K.; Choulis, S.A. Synergistic effects of buffer layer processing additives for enhanced hole carrier selectivity in inverted organic photovoltaics. *Org. Electron.* **2013**, *14*, 3123–3130.
69. Lu, H.; Akgun, B.; Russell, T.P. Morphological characterization of a low-bandgap crystalline polymer:PCBM bulk heterojunction solar cells. *Adv. Energy Mater.* **2011**, *1*, 870–878.
70. Waldauf, C.; Scharber, M.C.; Schilinsky, P.; Hauch, J.A.; Brabec, C.J. Physics of organic bulk heterojunction devices for photovoltaic applications. *J. Appl. Phys.* **2006**, *99*, 104503.
71. Steim, R.; Choulis, S.A.; Schilinsky, P.; Brabec, C.J. Interface modification for highly efficient organic photovoltaics. *Appl. Phys. Lett.* **2008**, *92*, 093303.
72. Lilliedal, M.R.; Medford, A.J.; Madsen, M.V.; Norrman, K.; Krebs, F.C. The effect of post-processing treatments on inflection points in current–voltage curves of roll-to-roll processed polymer photovoltaics. *Sol. Energy Mater. Sol. Cells* **2010**, *94*, 2018–2031.
73. Kim, J.; Kim, G.; Choi, Y.; Lee, J.; Heum Park, S.; Lee, K. Light-soaking issue in polymer solar cells: Photoinduced energy level alignment at the sol-gel processed metal oxide and indium tin oxide interface. *J. Appl. Phys.* **2012**, *111*, 114511.
74. Choi, H.; Lee, J.; Lee, W.; Ko, S.J.; Yang, R.; Lee, J.C.; Woo, H.Y.; Yang, C.; Kim, J.Y. Acid-functionalized fullerenes used as interfacial layer materials in inverted polymer solar cells. *Org. Electron.* **2013**, *14*, 3138–3145.
75. Goh, C.; Scully, S.R.; McGehee, M.D. Effects of molecular interface modification in hybrid organic-inorganic photovoltaic cells. *J. Appl. Phys.* **2007**, *101*, 114503.

76. Hsieh, C.H.; Cheng, Y.J.; Li, P.J.; Chen, C.H.; Dubosc, M.; Liang, R.M.; Hsu, C.S. Highly efficient and stable inverted polymer solar cells integrated with a cross-linked fullerene material as an interlayer. *J. Am. Chem. Soc.* **2010**, *132*, 4887–4893.
77. Chang, C.Y.; Wu, C.E.; Chen, S.Y.; Cui, C.; Cheng, Y.J.; Hsu, C.S.; Wang, Y.L.; Li, Y. Enhanced performance and stability of a polymer solar cell by incorporation of vertically aligned, cross-linked fullerene nanorods. *Angew. Chem. Int. Ed.* **2011**, *50*, 9386–9390.
78. Cheng, Y.J.; Hsieh, C.H.; He, Y.; Hsu, C.S.; Li, Y. Combination of indene-C60 bis-adduct and cross-linked fullerene interlayer leading to highly efficient inverted polymer solar cells. *J. Am. Chem. Soc.* **2010**, *132*, 17381–17383.
79. Cheng, Y.J.; Cao, F.Y.; Lin, W.C.; Chen, C.H.; Hsieh, C.H. Self-assembled and cross-linked fullerene interlayer on titanium oxide for highly efficient inverted polymer solar cells. *Chem. Mater.* **2011**, *23*, 1512–1518.
80. Hasegawa, T.; Miura, S.; Moriyama, T.; Kimura, T.; Takaya, I.; Osato, Y.; Mizutani, H. Novel Electron-Injection Layers for Top-Emission OLEDs. *Dig. Tech. Papers—Soc. Inf. Disp. Int. Symp.* **2004**, *35*, 154.
81. Liao, H.H.; Chen, L.M.; Xu, Z.; Li, G.; Yang, Y. Highly efficient inverted polymer solar cell by low temperature annealing of Cs_2CO_3 interlayer. *Appl. Phys. Lett.* **2008**, *92*, 173303.
82. Xin, Y.; Wang, Z.; Xu, L.; Xu, X.; Liu, Y.; Zhang, F. UV-Ozone treatment on Cs_2CO_3 interfacial layer for the improvement of inverted polymer solar cells. *J. Nanomater.* **2013**, *2013*, doi:10.1155/2013/104825.
83. Barbot, A.; Lucas, B.; di Bin, C.; Ratier, B.; Aldissi, M. Optimized inverted polymer solar cells incorporating Cs_2CO_3-doped C60 as electron transport layer. *Appl. Phys. Lett.* **2013**, *102*, 193305.
84. Cheng, G.; Tong, W.Y.; Low, K.H.; Che, C.M. Thermal-annealing-free inverted polymer solar cells using ZnO/Cs_2CO_3 bilayer as electron-selective layer. *Sol. Energy Mater. Sol. Cells* **2012**, *103*, 164–170.
85. Barbot, A.; Bin, C.; Lucas, B.; Ratier, B.; Aldissi, M. N-type doping and thermoelectric properties of co-sublimed cesium-carbonate-doped fullerene. *J. Mater. Sci.* **2013**, *48*, 2785–2789.
86. Yang, H.B.; Dong, Y.Q.; Wang, X.; Khoo, S.Y.; Liu, B.; Li, C.M. Graphene quantum dots-incorporated cathode buffer for improvement of inverted polymer solar cells. *Sol. Energy Mater. Sol. Cells* **2013**, *117*, 214–218.
87. Wiranwetchayan, O.; Liang, Z.; Zhang, Q.; Cao, G.; Singjai, P. The role of oxide thin layer in inverted structure polymer solar cells. *Mater. Sci. Appl.* **2011**, *2*, 1697–1701.
88. Lenzmann, F.; Krueger, J.; Burnside, S.; Brooks, K.; Grätzel, M.; Gal, D.; Rühle, S.; Cahen, D. Surface photovoltage spectroscopy of dye-sensitized solar cells with TiO2, Nb2O5, and SrTiO3 nanocrystalline photoanodes: Indication for electron injection from higher excited dye states. *J. Phys. Chem. B* **2001**, *105*, 6347–6352,
89. Li, Z.; Dong, Q.; Li, Y.; Xu, B.; Deng, M.; Pei, J.; Zhang, J.; Chen, F.; Wen, S.; Gao, Y.; Tian, W. Design and synthesis of solution processable small molecules towards high photovoltaic performance. *J. Mater. Chem.* **2011**, *21*, 2159–2168.

90. Wu, Y.; Zhang, W.; Li, X.; Min, C.; Jiu, T.; Zhu, Y.; Dai, N.; Fang, J. Solution-processed hybrid cathode interlayer for inverted organic solar cells. *ACS Appl. Mater. Interfaces* **2013**, *5*, 10428–10432.
91. Jin, S.H.; Jun, G.H.; Hong, S.H.; Jeon, S. Conformal coating of titanium suboxide on carbon nanotube networks by atomic layer deposition for inverted organic photovoltaic cells. *Carbon* **2012**, *50*, 4483–4488.
92. Kohlstadt, M.; Grein, M.; Reinecke, P.; Kroyer, T.; Zimmermann, B.; Würfel, U. Inverted ITO- and PEDOT:PSS-free polymer solar cells with high power conversion efficiency. *Sol. Energy Mater. Sol. Cells* **2013**, *117*, 98–102.
93. Oo, T.Z.; Chandra, R.D.; Yantara, N.; Prabhakar, R.R.; Wong, L.H.; Mathews, N.; Mhaisalkar, S.G. Zinc Tin Oxide (ZTO) electron transporting buffer layer in inverted organic solar cell. *Org. Electron.* **2012**, *13*, 870–874.
94. Kim, J.B.; Kim, C.S.; Kim, Y.S.; Loo, Y.L. Oxidation of silver electrodes induces transition from conventional to inverted photovoltaic characteristics in polymer solar cells. *Appl. Phys. Lett.* **2009**, *95*, 183301.
95. Chen, S.; Zhao, Y.; Cheng, G.; Li, J.; Liu, C.; Zhao, Z.; Jie, Z.; Liu, S. Improved light outcoupling for phosphorescent top-emitting organic light-emitting devices. *Appl. Phys. Lett.* **2006**, *88*, 153517.
96. Tao, C.; Ruan, S.; Zhang, X.; Xie, G.; Shen, L.; Kong, X.; Dong, W.; Liu, C.; Chen, W. Performance improvement of inverted polymer solar cells with different top electrodes by introducing a MoO3 buffer layer. *Appl. Phys. Lett.* **2008**, *93*, 193307.
97. Tao, C.; Ruan, S.; Xie, G.; Kong, X.; Shen, L.; Meng, F.; Liu, C.; Zhang, X.; Dong, W.; Chen, W. Role of tungsten oxide in inverted polymer solar cells. *Appl. Phys. Lett.* **2009**, *94*, 043311.
98. Servaites, J.D.; Ratner, M.A.; Marks, T.J. Organic solar cells: A new look at traditional models. *Energy Environ. Sci.* **2011**, *4*, 4410–4422.
99. Carter, S.A.; Angelopoulos, M.; Karg, S.; Brock, P.J.; Scott, J.C. Polymeric anodes for improved polymer light-emitting diode performance. *Appl. Phys. Lett.* **1997**, *70*, 2067–2069.
100. Kemerink, M.; Timpanaro, S.; de Kok, M.M.; Meulenkamp, E.A.; Touwslager, F.J. Three-dimensional inhomogeneities in PEDOT:PSS films. *J. Phys. Chem. B* **2004**, *108*, 18820–18825.
101. Ionescu-Zanetti, C.; Mechler, A.; Carter, S.; Lal, R. Semiconductive polymer blends: Correlating structure with transport properties at the nanoscale. *Adv. Mater.* **2004**, *16*, 385–389.
102. Stubhan, T.; Oh, H.; Pinna, L.; Krantz, J.; Litzov, I.; Brabec, C.J. Inverted organic solar cells using a solution processed aluminum-doped zinc oxide buffer layer. *Org. Electron.* **2011**, *12*, 1539–1543.
103. Lipomi, D.J.; Tee, B.C.K.; Vosgueritchian, M.; Bao, Z. Stretchable organic solar cells. *Adv. Mater.* **2011**, *23*, 1771–1775.
104. Baek, W.H.; Choi, M.; Yoon, T.S.; Lee, H.H.; Kim, Y.S. Use of fluorine-doped tin oxide instead of indium tin oxide in highly efficient air-fabricated inverted polymer solar cells. *Appl. Phys. Lett.* **2010**, *96*, 133506.

105. Heo, S.W.; Baek, K.H.; Lee, T.H.; Lee, J.Y.; Moon, D.K. Enhanced performance in inverted polymer solar cells via solution process: Morphology controlling of PEDOT:PSS as anode buffer layer by adding surfactants. *Org. Electron.* **2013**, *14*, 1629–1635.
106. Lim, F.J.; Ananthanarayanan, K.; Luther, J.; Ho, G.W. Influence of a novel fluorosurfactant modified PEDOT:PSS hole transport layer on the performance of inverted organic solar cells. *J. Mater. Chem.* **2012**, *22*, 25057–25064.
107. Gupta, D.; Wienk, M.M.; Janssen, R.A.J. Efficient polymer solar cells on opaque substrates with a laminated PEDOT:PSS top electrode. *Adv. Energy Mater.* **2013**, *3*, 782–787.
108. Suh, Y.; Lu, N.; Lee, S.H.; Chung, W.S.; Kim, K.; Kim, B.; Ko, M.J.; Kim, M.J. Degradation of a thin Ag layer induced by poly(3,4-ethylenedioxythiophene):polystyrene sulfonate in a transmission electron microscopy specimen of an inverted polymer solar cell. *ACS Appl. Mater. Interfaces* **2012**, *4*, 5118–5124.
109. Meyer, J.; Hamwi, S.; Bülow, T.; Johannes, H.H.; Riedl, T.; Kowalsky, W. Highly efficient simplified organic light emitting diodes. *Appl. Phys. Lett.* **2007**, *91*, 113506.
110. Wang, F.; Qiao, X.; Xiong, T.; Ma, D. The role of molybdenum oxide as anode interfacial modification in the improvement of efficiency and stability in organic light-emitting diodes. *Org. Electron.* **2008**, *9*, 985–993.
111. Tokito, S.; Noda, K.; Taga, Y. Metal oxides as a hole-injecting layer for an organic electroluminescent device. *J. Phys. D* **1996**, *29*, 2750–2753.
112. Yin, Z.; Zheng, Q.; Chen, S.C.; Cai, D. Interface control of semiconducting metal oxide layers for efficient and stable inverted polymer solar cells with open-circuit voltages over 1.0 volt. *ACS Appl. Mater. Interfaces* **2013**, *5*, 9015–9025.
113. Chambon, S.; Derue, L.; Lahaye, M.; Pavageau, B.; Hirsch, L.; Wantz, G. MoO3 thickness, thermal annealing and solvent annealing effects on inverted and direct polymer photovoltaic solar cells. *Materials* **2012**, *5*, 2521–2536.
114. Ng, A.; Liu, X.; To, C.H.; Djurišić, A.B.; Zapien, J.A.; Chan, W.K. Annealing of P3HT:PCBM blend film—The effect on its optical properties. *ACS Appl. Mater. Interfaces* **2013**, *5*, 4247–4259.
115. Dupont, S.R.; Oliver, M.; Krebs, F.C.; Dauskardt, R.H. Interlayer adhesion in roll-to-roll processed flexible inverted polymer solar cells. *Sol. Energy Mater. Sol. Cells* **2012**, *97*, 171–175.
116. Kundu, S.; Gollu, S.R.; Sharma, R.; G, S.; Ashok, A.; Kulkarni, A.; Gupta, D. Device stability of inverted and conventional bulk heterojunction solar cells with MoO3 and ZnO nanoparticles as charge transport layers. *Org. Electron.* **2013**, *14*, 3083–3088.
117. Elumalai, N.K.; Saha, A.; Vijila, C.; Jose, R.; Jie, Z.; Ramakrishna, S. Enhancing the stability of polymer solar cells by improving the conductivity of the nanostructured MoO3 hole-transport layer. *Phys. Chem. Chem. Phys.* **2013**, *15*, 6831–6841.
118. Pan, H.; Zuo, L.; Fu, W.; Fan, C.; Andreasen, B.; Jiang, X.; Norrman, K.; Krebs, F.C.; Chen, H. MoO3–Au composite interfacial layer for high efficiency and air-stable organic solar cells. *Org. Electron.* **2013**, *14*, 797–803.
119. Lampande, R.; Kim, G.W.; Boizot, J.; Kim, Y.J.; Pode, R.; Kwon, J.H. A highly efficient transition metal oxide layer for hole extraction and transport in inverted polymer bulk heterojunction solar cells. *J. Mater. Chem. A* **2013**, *1*, 6895–6900.

120. Stubhan, T.; Li, N.; Luechinger, N.A.; Halim, S.C.; Matt, G.J.; Brabec, C.J. High fill factor polymer solar cells incorporating a low temperature solution processed WO3 hole extraction layer. *Adv. Energy Mater.* **2012**, *2*, 1433–1438.
121. Zilberberg, K.; Trost, S.; Meyer, J.; Kahn, A.; Behrendt, A.; Ltzenkirchen-Hecht, D.; Frahm, R.; Riedl, T. Inverted organic solar cells with sol-gel processed high work-function vanadium oxide hole-extraction layers. *Adv. Funct. Mater.* **2011**, *21*, 4776–4783.
122. Yu, W.; Shen, L.; Ruan, S.; Meng, F.; Wang, J.; Zhang, E.; Chen, W. Performance improvement of inverted polymer solar cells thermally evaporating nickel oxide as an anode buffer layer. *Sol. Energy Mater. Sol. Cells* **2012**, *98*, 212–215.
123. Lim, D.C.; Kim, Y.T.; Shim, W.H.; Jang, A.Y.; Lim, J.H.; Kim, Y.D.; Jeong, Y.; Kim, Y.D.; Lee, K.H. Wet-chemically prepared NiO layers as hole transport layer in the inverted organic solar cell. *Bull. Korean Chem. Soc.* **2011**, *32*, 1067–1070.
124. Huang, J.S.; Chou, C.Y.; Lin, C.F. Efficient and air-stable polymer photovoltaic devices with WO3-V2O5 mixed oxides as anodic modification. *IEEE Electron Device Lett.* **2010**, *31*, 332–334.
125. Shelton, S.W.; Chen, T.L.; Barclay, D.E.; Ma, B. Solution-processable triindoles as hole selective materials in organic solar cells. *ACS Appl. Mater. Interfaces* **2012**, *4*, 2534–2540.
126. Liu, J.; Xue, Y.; Gao, Y.; Yu, D.; Durstock, M.; Dai, L. Hole and electron extraction layers based on graphene oxide derivatives for high-performance bulk heterojunction solar cells. *Adv. Mater.* **2012**, *24*, 2228–2233.
127. Allen, M.J.; Tung, V.C.; Kaner, R.B. Honeycomb carbon: A review of graphene. *Chem. Rev.* **2010**, *110*, 132–145.
128. Yao, K.; Chen, L.; Chen, X.; Chen, Y. Self-organized hole transport layers based on polythiophene diblock copolymers for inverted organic solar cells with high efficiency. *Chem. Mater.* **2013**, *25*, 897–904.
129. Greiner1, M.T.; Lu, Z.H. Thin-film metal oxides in organic semiconductor devices: Their electronic structures, work functions and interfaces. *NPG Asia Mater.* **2013**, *5*, e55.
130. Xie, F.; Choy, W.C.H. Hydrogen metal oxide bronzes for efficient hole transport layers. *SPIE Newsroom* **2013**, doi:10.1117/2.1201311.005133.
131. Stubhan, T.; Ameri, T.; Salinas, M.; Krantz, J.; Machui, F.; Halik, M.; Brabec, C.J. High shunt resistance in polymer solar cells comprising a MoO3 hole extraction layer processed from nanoparticle suspension. *Appl. Phys. Lett.* **2011**, *98*, 253308.
132. Choi, H.; Kim, B.; Ko, M.J.; Lee, D.K.; Kim, H.; Kim, S.H.; Kim, K. Solution processed {WO3} layer for the replacement of PEDOT:PSS layer in organic photovoltaic cells. *Org. Electron.* **2012**, *13*, 959–968.
133. Li, N.; Stubhan, T.; Luechinger, N.A.; Halim, S.C.; Matt, G.J.; Ameri, T.; Brabec, C.J. Inverted structure organic photovoltaic devices employing a low temperature solution processed {WO3} anode buffer layer. *Org. Electron.* **2012**, *13*, 2479–2484.
134. Li, N.; Stubhan, T.; Baran, D.; Min, J.; Wang, H.; Ameri, T.; Brabec, C.J. Design of the solution-processed intermediate layer by engineering for inverted organic multi junction solar cells. *Adv. Energy Mater.* **2013**, *3*, 301–307.

135. Yip, H.L.; Jen, A.K.Y. Recent advances in solution-processed interfacial materials for efficient and stable polymer solar cells. *Energy Environ. Sci.* **2012**, *5*, 5994–6011.
136. Angmo, D.; Gonzalez-Valls, I.; Veenstra, S.; Verhees, W.; Sapkota, S.; Schiefer, S.; Zimmermann, B.; Galagan, Y.; Sweelssen, J.; Lira-Cantu, M.; *et al*. Low-cost upscaling compatibility of five different ITO-free architectures for polymer solar cells. *J. Appl. Polym. Sci.* **2013**, *130*, 944–954.
137. Voroshazi, E.; Cardinaletti, I.; Uytterhoeven, G.; Shan, L.; Empl, M.; Aernouts, T.; Rand, B.P. Role of electron- and hole-collecting buffer layers on the stability of inverted polymer: Fullerene photovoltaic devices. *IEEE J. Photovolt.* **2014**, *4*, 265–270.
138. Lizin, S.; van Passel, S.; de Schepper, E.; Maes, W.; Lutsen, L.; Manca, J.; Vanderzande, D. Life cycle analyses of organic photovoltaics: A review. *Energy Environ. Sci.* **2013**, *6*, 3136–3149.
139. Espinosa, N.; Hosel, M.; Angmo, D.; Krebs, F.C. Solar cells with one-day energy payback for the factories of the future. *Energy Environ. Sci.* **2012**, *5*, 5117–5132.
140. Espinosa, N.; Garcia-Valverde, R.; Krebs, F.C. Life-cycle analysis of product integrated polymer solar cells. *Energy Environ. Sci.* **2011**, *4*, 1547–1557.